Guidelines for the Selection of Scintillators for Indirect Photon-Counting X-ray Detectors

van Blaaderen, J. Jasper; van Aarle, Casper; Leibold, David; Dorenbos, Pieter; Schaart, Dennis R.

DOI
10.1021/acs.chemmater.4c03437

Publication date
2025

Document Version
Final published version

Published in
Chemistry of Materials

CHEMISTRY OF MATERIALS

pubs.acs.org/cm

Perspective

Guidelines for the Selection of Scintillators for Indirect Photon-Counting X-ray Detectors

J. Jasper van Blaaderen,* Casper van Aarle, David Leibold, Pieter Dorenbos, and Dennis R. Schaart*

Cite This: *Chem. Mater.* 2025, 37, 1716−1740

Read Online

ACCESS | Metrics & More | Article Recommendations | Supporting Information

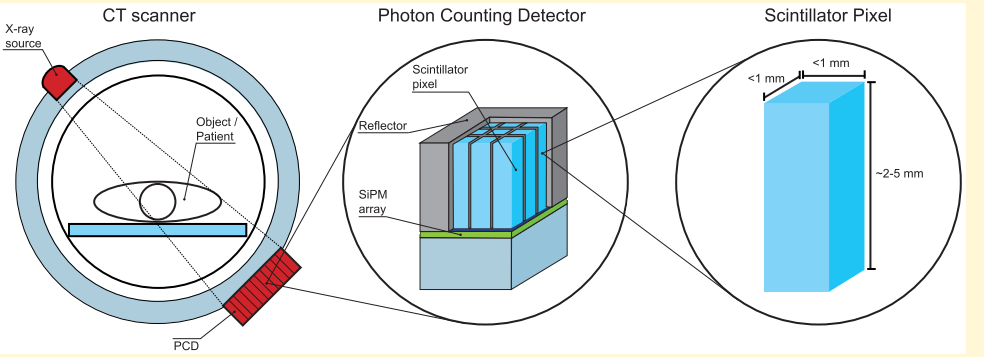

ABSTRACT: X-ray photon-counting detectors (PCDs) are a rapidly developing technology. Current PCDs used in medical imaging are based on CdTe, CZT, or Si semiconductor detectors, which directly convert X-ray photons into electrical pulses. An alternative approach is to combine ultrafast scintillators with silicon photomultipliers (SiPMs). Here, an overview is presented of different classes of scintillators, with the aim of assessing their potential application in scintillator-SiPM based indirect X-ray PCDs. To this end, three figures of merit (FOMs) are defined: the pulse intensity, the pulse duration, and the pulse quality. These FOMs quantify how characteristics such as light yield, pulse shape, and energy resolution affect the suitability of scintillators for application in indirect PCDs. These FOMs are based on emissive characteristics; a fourth FOM ($\rho Z_{eff}^{3.5}$) is used to also take stopping power into account. Other important properties for the selection process include low self-absorption, low after-glow, possibility to produce sub-mm pitch pixel arrays, and cost-effectiveness. It is shown that material classes with promising emission properties are Ce^{3+}- or Pr^{3+}-doped materials, near band gap exciton emitters, plastics, and core−valence materials. Possible shortcomings of each of these groups, e.g., suboptimal emission wavelength, nonproportionality, and density, are discussed. Additionally, the engineering approach of quenching the scintillator emission, resulting in a targeted shortening of the decay time, and the possibility of codoping are explored. When selecting and/or engineering a material, it is important to consider not only the characteristics of the scintillator but also relevant SiPM properties, such as recharge time and photodetection efficiency.

I. INTRODUCTION

X-ray computed tomography (CT) is a widely used medical imaging technique. Most CT scanners today use a pixelated energy-integrating detector (EID), which yields a signal proportional to the total energy deposited in each pixel during the exposure time. As a result, no discrimination is made between the energy of incident X-rays, with high-energy X-rays contributing more to the signal. Moreover, electronic noise is integrated during the exposure time. EIDs are thus limited in signal-to-noise and contrast-to-noise ratio for a given radiation dose.[1,2]

Photon-counting detectors (PCDs) can help mitigate these problems. A PCD counts the number of incident X-ray photons hitting the detector during the exposure time, only registering a count when the electrical output pulse of the PCD passes a predefined threshold. As a result, most of the electronic noise is rejected. In the case of a purely counting detector, all X-ray photons contribute equally to the detector signal. The use of multiple thresholds makes it possible to assign counts to different energy bins, thus yielding an energy-resolving PCD, which enables the use of PCDs in dual- or multienergy (spectral) X-ray imaging.

Despite their advantages, PCDs are thus far not widely implemented in medical X-ray imaging systems. One of the challenges to their implementation is the high X-ray fluence rates that occur in medical imaging. Due to the detector's finite response time, multiple X-ray photons hitting a pixel within this

Received: December 17, 2024
Revised: February 11, 2025
Accepted: February 12, 2025
Published: February 26, 2025

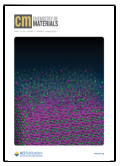

https://doi.org/10.1021/acs.chemmater.4c03437
Chem. Mater. 2025, 37, 1716−1740

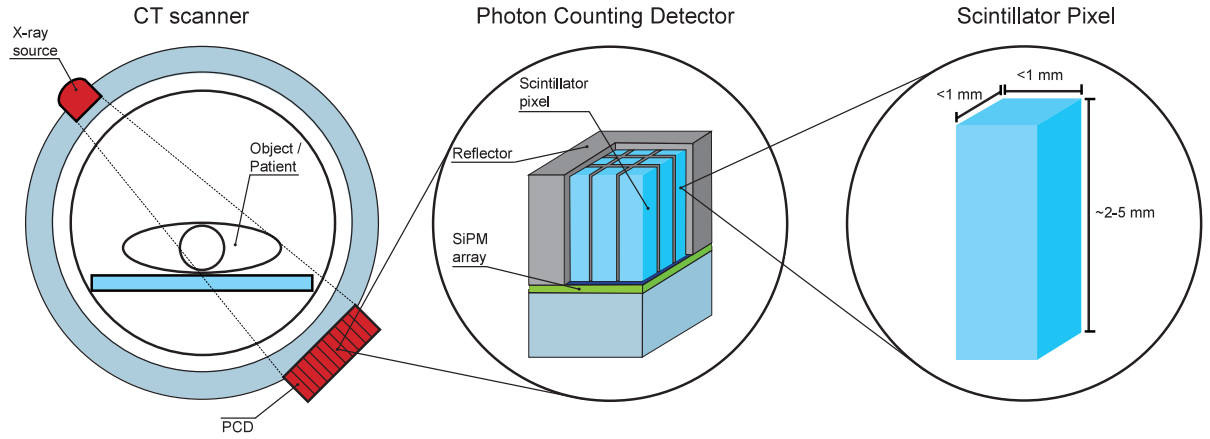

Figure 1. Schematic overview of, from left to right, a simplified photon-counting CT set up, a simplified overview of the pixilated PCD for which part of the reflector is removed to show the scintillator pixels, and one of the scintillator pixels with the approximate crystal size.

response time result in a superposition of their respective electrical output pulses. This is termed pulse pile-up. It can lead to the registration of a count in an energy bin with an energy higher than the incident X-ray photon's energy. It has been estimated by Persson et al. that the maximum fluence rate reached in a standard clinical CT protocol is approximately 3.4×10^8 photons/s/mm^2; however, the fluence rate in most regions of a patient's shadow on the detector are much lower than the maximum.[3] In order to be able to handle this fluence rate and to reduce pulse pile-up, the detector pulse duration should not exceed more than a few tens of nanoseconds. Additionally, miniaturization of the pixels, to a size smaller than 0.5×0.5 mm^2, helps to distribute the incident photons over multiple pixels, reducing the rate requirement per pixel. This does, however, increase the probability that a characteristic or Compton scattered X-ray photon escapes from a pixel and is absorbed in a neighboring pixel. This is referred to as interpixel X-ray crosstalk and increases pulse pile-up and reduces spatial resolution.[4] Further requirements for PCDs are a sufficient full width at half-maximum (fwhm) energy resolution of the detector system in the diagnostic energy range (25 to 150 keV), sufficient density to achieve high X-ray stopping power, and room temperature operation.

The potential of PCDs for CT has been explored extensively in the last 10 years.[1,5−8] Current PCDs are based on direct detection, converting the energy deposited by X-ray photons into a charge pulse using semiconductors such as CdTe,[9] $Cd_{1-x}Zn_xTe$ (CZT),[10] or Si.[11] Several photon-counting CT systems have been constructed and are being used to evaluate their benefits in clinical practice.[1,12] These systems can reach energy resolutions in the range of 10 to 20% at 60 keV.[10,13] Nevertheless, CdTe- and CZT-based PCDs face several challenges, for example, the production of detector-grade semiconductors with sufficiently low defect density,[1,2] which can affect cost-effectiveness. Another challenge is the occurrence of charge sharing between pixels,[10] which leads to errors in both the number of registered counts and their energies.[14] Additionally the low hole mobility of CdTe and CZT can give result in polarization effects at high count rates.[1] Additionally, the effects of long-term exposure to the high X-ray fluence rates on detector performance of CdTe and CZT-based detectors is yet to be investigated.[5] For Si-based detectors, the low atomic number ($Z = 14$) and density ($\rho = 2.3$ g/cm^3) makes Compton scattering the dominant interaction mechanism of X-ray photons[4] within the pixels, degrading both spectral performance and spatial resolution.[15]

An alternative to the above-mentioned direct PCDs are indirect detectors, utilizing ultrafast scintillators to absorb the incident X-rays and convert them into scintillation photons. Scintillators have proven to be reliable and cost-effective detector materials in a plethora of medical imaging systems, including positron emission tomography (PET), single-photon emission tomography (SPECT), and energy-integrating CT systems.[16−21] Moreover, scintillators do not suffer from polarization or charge sharing effects. Therefore, indirect PCDs may perform better in spectral imaging tasks.[14] The scintillation photons are detected and converted into an electrical pulse using a photodetector. A simplified schematic of a scintillator based, or indirect, PCD is shown in Figure 1. From left to right, it shows a simplified photon-counting CT set up, a pixelated PCD, and a single scintillator pixel crystal. In an indirect PCD, the scintillator pixels are separated and covered on the outside by reflectors in order to efficiently collect the scintillation photons and avoid optical crosstalk between pixels. Part of the outside reflector is removed in the diagram to show the scintillator pixels underneath. In this work, the focus will be on the use of silicon photomultipliers (SiPMs) as the photodetectors, due to their internal gain, short response time, compactness, robustness, and the possibility to implement sub-mm pixel sizes.[22−25] A SiPM pixel consists of a two-dimensional (2D) array of single-photon avalanche diodes (SPADs) with a size on the order of 10 μm. When a photon hits a SPAD, an avalanche of charge carriers is created. Since the SPADs within a SiPM are connected in parallel, the output signal is proportional to the number of scintillation photons incident on the SiPM, provided that the number of SPADs is sufficiently large compared to the number of scintillation photons. The SiPM should have a short recharge time and a photodetection efficiency curve matching the emission spectrum of the scintillator.

In an indirect PCD, the scintillator should have a sufficiently high density to efficiently absorb the incident X-rays and minimize X-ray cross-talk between pixels. The scintillator should also have a short decay time in order to handle high X-ray fluence rates. Initial feasibility studies on SiPM-based scintillator PCDs have been performed by Van der Sar et al. by coupling $(Lu_{1-x}Y_x)_2SiO_5:Ce^{3+}$ (LYSO:Ce^{3+}), $YAlO_3:Ce^{3+}$ (YAP:Ce^{3+}), $LuAlO_3:Ce^{3+}$ (LAP:Ce^{3+}), and $LaBr_3:Ce^{3+}$ to a single-pixel

https://doi.org/10.1021/acs.chemmater.4c03437
Chem. Mater. 2025, 37, 1716−1740

SiPM with a recharge time of 7 ns.[22−25] The pulse duration, defined as the fwhm of the detector output pulse, of the $LaBr_3$:Ce^{3+} based detector was experimentally determined to be 26.5 ns fwhm.[23] Using the same definition, the pulse duration of a typical CdTe-based detector is 14 ns fwhm.[14] Additionally, a fwhm energy resolution of 8% at 60 kV has been demonstrated for CdTe-based PCDs.[10] Experimentally, the $LaBr_3$:Ce^{3+}-based detector showed a fwhm energy resolution of 20% at 60 keV.[22,24,25] In those studies, however, the energy resolution was limited by the low (<25%) photodetection efficiency of the used SiPM. It has been demonstrated by Alekhin et al. that $LaBr_3$:Ce^{3+} can reach an energy resolution of 9.4% at 60 keV.[26]

Another study, by Arimoto et al., used a 1 × 64 array of 1 × 1 mm^2 pixels coupled to a cerium-doped yttrium−gadolinium−aluminum−gallium garnet (YGAGG) scintillator.[27] Arimoto et al. demonstrated that, with an energy resolution of 32% at 60 keV, it was possible to acquire energy-resolved X-ray images and perform material decomposition.[28,29] However, the X-ray fluence rate was restricted by the 70 ns decay time of the YGAGG scintillator. Sato et al. also used YGAGG to construct a table-top preclinical CT system, demonstrating accurate density maps of gadolinium and iodine.[30] Another example is the work of Shimazoe et al., who build a pixelated detector based on gadolinium−aluminum−gallium garnet (GAGG)/gadolinium−fine aluminum−gallate (GFAG) scintillator pixels coupled to a finely pixelated SiPM array.[31] The detector consisted of a 10 × 10 scintillator pixel array of 200 μm^2 separated by a optical reflection layer with a thickness of 50 μm. The scintillators used in this detector, (GAGG)/(GFAG), have decay times of more than 50 ns, restricting the range of fluence rates under which the detector can operate.

In this work, an overview of different types of scintillators is presented. The goal is to identify suitable materials for use in indirect PCDs. To this end, three different figures of merit (FOMs) are formulated: the pulse intensity, the pulse duration, and the pulse quality. These FOMs aim to quantify how scintillator emissive characteristics such as light yield, pulse shape, and energy resolution affect the suitability of the material for application in indirect PCDs. Additionally, a fourth FOM is used to assess the X-ray stopping power of the material. Next to the presented material selection, potential challenges for different classes of scintillators are identified. The presented framework is also used to explore the possibility of engineering a scintillator for use in an indirect PCD.

II. SIGNAL FORMATION IN AN INDIRECT PCD

In order to assess how the emission characteristics of different scintillators influence the performance of an indirect PCD, a simple model has been formulated. The model describes how the essential parts of the detection chain affect the signal formation, taking into account properties of both the scintillation crystal and the SiPM. The model can be subdivided into four different stages, from the generation of X-ray photons to the electrical output pulse of the indirect PCD.

II.A. Stage I. In the first stage, an X-ray photon is created and passes through the object, e.g., a patient. After this, the X-ray photon with energy E_X impinged on a pixel of the detector. It then either interacts with the scintillator or passes through without depositing any energy. The probability of interaction is determined by the density and elemental composition of the scintillation material, as well as the pixel dimensions.

In case the X-ray photon interacts, it deposits an amount of energy E_{dep} in the scintillator-pixel. E_{dep} is not always the same as E_X and depends on the probability of secondary photons, i.e., Compton scattered photons, or characteristic X-rays, escaping the pixel. These probabilities again depend on the material density and composition, as well as the dimensions of the pixel and the location of interaction of the X-ray photon within it.

II.B. Stage II. In the second stage, the energy deposited by the interacting X-ray is converted to a flash of scintillation photons. The average number of emitted scintillations photons for a given amount of deposited energy is given by

$$\overline{N}_{em} = Y_{E\gamma} \cdot r_{np}(E_{dep}) \cdot E_{dep} \tag{1}$$

Here, $Y_{E\gamma}$ represents the light yield of the scintillator per unit of energy for a given amount of deposited energy, often 662 keV from γ-photons of ^{137}Cs. Ideally, the light yield would be independent of the amount of deposited energy. In reality, however, this is not the case. The relative variation of the light yield with deposited energy is called nonproportionality and is represented by the term $r_{np}(E_{dep})$. A more elaborate discussion of the role of nonproportionality is provided in Section III.A.

II.C. Stage III. In the third stage, the scintillation photons are transported through the crystal toward the SiPM where each photon may trigger a SPAD, in which case it is detected. The expected number of detected scintillaton photons ($\overline{N}_{det}$) is given by

$$\overline{N}_{det} = \overline{N}_{em} \cdot \overline{\eta}_{det} \tag{2}$$

Here, $\overline{\eta}_{det}$ represents the effective photon detection efficiency (PDE) of the detector. The effective PDE is defined as

$$\overline{\eta}_{det} = \int_0^\infty \lambda_{em}(\lambda) \cdot \eta_{ot}(\lambda) \cdot \eta_{pd}(\lambda) d\lambda \tag{3}$$

Here, $\lambda_{em}(\lambda)$ represents the emission spectrum of the scintillator, normalized according to

$$\int_0^\infty \lambda_{em}(\lambda) d\lambda = 1 \tag{4}$$

while $\eta_{ot}(\lambda)$ is the optical transfer efficiency of the detector (taking into account e.g. the optical properties of the scintillator and optical coupling material, the reflectivity of the reflectors, etc.), and $\eta_{pd}(\lambda)$ is the photon detection efficiency of the SiPM. The effective PDE thus depends on properties of the scintillator, the photodetector, and any other relevant components of the detector.

II.D. Stage IV. In the fourth and final stage, the SiPM generates an electrical pulse. In reality, the charge $Q(E_X)$ contained in this pulse depends not only on the number of detected scintillation photons but also on the nonproportional response of the SiPM due to saturation effects, afterpulsing, and crosstalk. The role of these effects on the response of a SiPM-based scintillation detector has been discussed comprehensively by van Dam et al.[32] In a well-designed detector, one attempts to mitigate these effects so as to obtain a response that is as proportional as reasonably achievable. Moreover, the acquired detector signals can be corrected for any remaining nonproportionality, for example using the model by van Dam et al.[32] For simplicity, we will therefore assume that $Q(E_X)$ is proportional to $\overline{N}_{det}$ in the remainder of this work.

The electrical output pulse of the detector can be described by convolution of the single SPAD response and the decay profile of the scintillation pulse. The response of a single fired SPAD can be approximated as an exponentially decaying current:

https://doi.org/10.1021/acs.chemmater.4c03437
Chem. Mater. 2025, 37, 1716−1740

$$I_{spad}(t) = \begin{cases} \frac{G}{\tau_{rech}} \cdot (e^{-t/\tau_{rech}}), & t \geq 0 \\ 0, & t < 0 \end{cases} \quad (5)$$

where G and τ_{rech} are the gain and the recharge time constant of the SiPM, respectively.

The expected time distribution of the emitted scintillation photons, on the other hand, can be described by

$$n_{em}(t) = \frac{\bar{N}_{em}}{\tau_{dec}\tau_{rise}} \cdot (e^{-t/\tau_{dec}} - e^{-t/\tau_{rise}}) \quad (6)$$

Here, τ_{rise} and τ_{dec} are the rise and decay time constants of the scintillator, respectively.

Due to the submillimeter size of the scintillator crystal, it can be assumed that the optical transfer times of the scintillation photons can be neglected. The time distribution of the number of triggered SPADs, i.e., the number of detected scintillation photons, can therefore be described to a good approximation by

$$n_{det}(t) = \bar{\eta}_{det} \cdot n_{em}(t) = \frac{\bar{N}_{det}}{\tau_{dec}\tau_{rise}} \cdot (e^{-t/\tau_{dec}} - e^{-t/\tau_{rise}}) \quad (7)$$

If the rise time is significantly shorter than the decay time, this result can be further simplified to

$$n_{det}(t) = \frac{\bar{N}_{det}}{\tau_{dec}} \cdot (e^{-t/\tau_{dec}}) \quad (8)$$

In reality, a measured scintillator decay curve may show nonexponential behavior or consist of multiple decay components. In order to still arrive at a simple model, such decay behavior can be approximated using a single exponential. In this work, a weighted average is used for the decay time constant in the case of multiple decay components. This is discussed more elaborately in Section IV and eq 16.

Following the above discussion, the time evolution of the detector output pulse can be calculated by convoluting eqs 5 and 8:

$$I_{det}(t) = \begin{cases} \frac{\bar{N}_{det}G}{\tau_{rech}\tau_{dec}} \cdot (e^{-t/\tau_{rech}} - e^{-t/\tau_{dec}}), & t \geq 0 \\ 0, & t < 0 \end{cases} \quad (9)$$

III. FIGURES OF MERIT

Based on the above discussion, three different FOMs can be formulated to quantify the performance potential of a scintillator in indirect PCDs. The FOMs are the pulse intensity, the pulse duration, and the pulse quality.

III.A. Pulse Intensity. The pulse intensity is simply defined as the expected number of detected scintillation photons, $\bar{N}_{det}$, defined in eq 2. As discussed in Section II.C, it depends on both $\bar{N}_{em}$ and $\bar{\eta}_{det}$ making it a property related to the scintillator, SiPM, and any other relevant components of the detector.

$\bar{N}_{det}$ is closely related to the energy resolution R of the detector. To explain this, we can make use of a formulation of the energy resolution of a scintillation detector that is frequently used in literature:[33−36]

$$R^2 = R_{stat}^2 + R_{np}^2 + R_{in}^2 \quad (10)$$

Here, R_{stat}^2 represents the statistical variance in the number of photons detected by the photon detector and R_{np}^2 the variance due to the nonproportionality of the scintillator. The variance due to crystal inhomogeneities influencing the energy resolution, e.g., a nonuniform distribution of dopant ions and/or surface effects, is represented by R_{in}^2. In an indirect PCD, the influence of R_{in}^2 is expected to be small due to the submillimeter size of the scintillation crystals. For completion, it is noted that eq 10 does not take into account electronic contributions as the focus of this work is on scintillation materials.

Nonproportionality, $r_{np}(E_{dep})$, is a material property describing the relative variation of the light yield $Y_{E\gamma}$ with deposited energy, referred to as the energy E_γ at which $Y_{E\gamma}$ was determined.[36,37] It has been studied extensively, both experimentally[38−41] and theoretically[42−45] in the last two decades. Traditionally, scintillator energy resolutions are determined using the 662 keV γ-photons of ^{137}Cs.[33] At this energy, nonproportionality tends to have a relatively large influence on the scintillator energy resolution, and consequently, the statistical limit of the energy resolution can only be reached when $r_{np}(E_{dep})$ is close to an ideal response, i.e., $r_{np}(E_{dep}) = 1$ for all values of E_{dep}. In the diagnostic energy range (25 to 150 keV), on the other hand, the dominant factor influencing the energy resolution is R_{stat}^2 (which is discussed in more detail below). This means that the energy resolution improves when the nonproportionality is larger than 1 in the diagnostic energy range. On the other hand, when the nonproportionality is smaller than 1, the energy resolution will deteriorate. Experimentally, this means that characterizing a scintillator using the 59.5 keV gamma photons of ^{241}Am instead of the 662 keV gamma photons of ^{137}Cs will provide much more relevant information with respect to their application in indirect PCDs.

The term R_{stat} depends on the number of detected scintillation photons. It can be described by a binomial distribution. In practice, however, it is commonly approximated by a Poisson distribution. Hence, assuming Poisson statistics,

$$R_{stat} \propto \sqrt{\frac{1}{\bar{N}_{det}}} \quad (11)$$

In case R_{in}, R_{np}, and all other contributions to the energy resolution can be considered negligible, eq 11 defines the lower limit on the energy resolution of a scintillator-based PCD. Theoretically, the best value of R_{stat} is achieved for $\bar{\eta}_{det} = 1$, resulting in $\bar{N}_{det} = \bar{N}_{em}$ (see eq 2). This means that each of the emitted scintillation photons reaches the SiPM and triggers a SPAD. In practice, $\bar{\eta}_{det} < 1$ and one attempts to maximize its value by optimizing the optical transfer efficiency of the detector and matching the PDE curve of the SiPM to the scintillator emission spectrum (see eq 3).

In summary, the energy resolution that can be achieved with an indirect PCD scales inversely proportional to the square root of the number of detected scintillation photons. Moreover, $\bar{N}_{det}$ should be evaluated in the diagnostic energy range, for example using 59.5 keV gamma photons of ^{241}Am, in order to take the nonproportionality of the scintillator into account.

III.B. Pulse Duration. The pulse duration (t_{fwhm}) is defined as the fwhm of the average detector output pulse $I_{det}(t)$. It is noted that we can facilitate the (numerical) calculation of the fwhm of eq 9, by first normalizing this function such that the peak value is always equal to one:[46,47]

$$I_{norm}(t) = \begin{cases} k \cdot (e^{-t/\tau_{rech}} - e^{-t/\tau_{dec}}), & t \geq 0 \\ 0, & t < 0 \end{cases} \quad (12)$$

https://doi.org/10.1021/acs.chemmater.4c03437
Chem. Mater. 2025, 37, 1716−1740

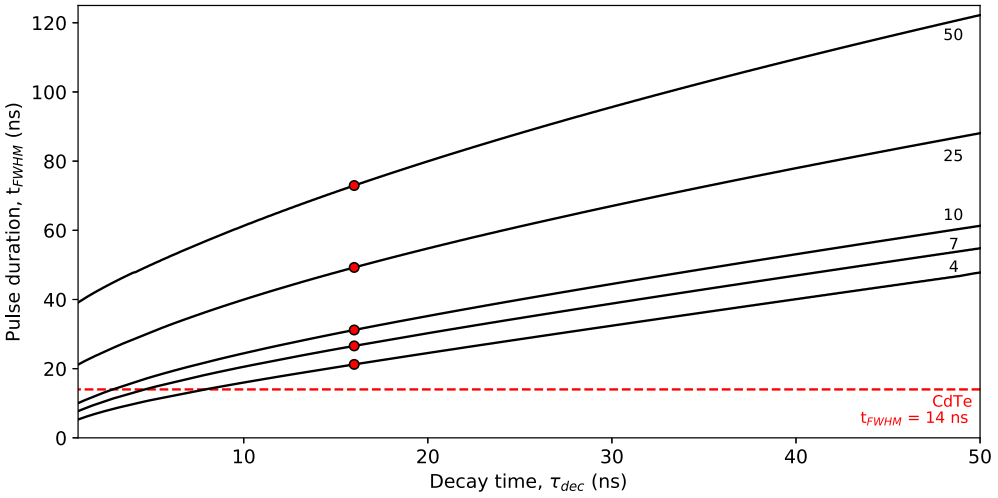

Figure 2. Calculated pulse duration (t_{fwhm}) as a function of the scintillator decay time (τ_{dec}) for different recharge times (τ_{rech}). The red dashed line represents a state-of-the-art-pulse duration of 14 ns fwhm of a CdTe detector. The red markers indicate the calculated pulse duration of a $LaBr_3$:Ce^{3+}-based PCD for different recharge times.

Here, the normalization constant k is defined as

$$k = [e^{-\alpha \ln(\alpha/\beta)/(\alpha-\beta)} - e^{-\beta \ln(\alpha/\beta)/(\alpha-\beta)}]^{-1} \quad (13)$$

where α and β are defined as $1/\tau_{rech}$ and $1/\tau_{dec}$, respectively.

Figure 2 shows the calculated pulse duration (t_{fwhm}) as a function of the scintillator decay time constant, for different recharge time constants ranging from 4 to 50 ns. For reference, the pulse duration of CdTe based detector, 14 ns fwhm, is indicated by the red dashed line.[14] Since several CdTe-based direct PCDs have been used to evaluate their use in clinical practice, it can be assumed that a pulse duration of at most 14 ns fwhm is sufficient to handle the high X-ray fluency rate of medical imaging systems.[1,12] As a second reference, red circular markers are added at 16 ns, which represent the decay time of $LaBr_3$:Ce^{3+}. For a SiPM with τ_{rech} = 7 ns, as was used experimentally by van der Sar et al.,[22−25] the calculated pulse duration of $LaBr_3$:Ce^{3+} is equal to 26.5 ns fwhm. Decreasing τ_{rech} to 4 ns reduces the pulse duration to 21.2 ns fwhm. This shows that further decreasing the recharge time of the SiPM only results in marginal improvement of the pulse duration of a $LaBr_3$:Ce^{3+}-based PCD due to the fact that a recharge time of 7 ns is already significantly shorter than the 16 ns scintillation decay time. The relative influence of τ_{rech} will be larger for a faster scintillator.

III.C. Pulse Quality. The pulse quality (PQ) is defined as

$$PQ = \sqrt{\frac{\bar{N}_{det}}{t_{fwhm}}} \quad (14)$$

This FOM equals the square root of the ratio of the pulse intensity and duration. In case $\tau_{dec} \ll \tau_{rech}$, the shape of $I_{det}(t)$ is mainly determined by τ_{rech} and can therefore be considered constant, see eq 9. The uncertainty in the amplitude of $I_{det}(t)$ is then determined by the Poisson variation of N_{det} and, therefore, inversely proportional with PQ. If, on the other hand, $\tau_{rech} \ll \tau_{dec}$, the average shape of $I_{det}(t)$ is mainly determined by τ_{dec}. In that case, a smaller value of PQ implies not only a larger uncertainty in the amplitude of $I_{det}(t)$, but also an increase of the statistical fluctuations in the shape of $I_{det}(t)$, due to the random emission times of the scintillation photons. If these statistical pulse shape fluctuations become too strong, a single pulse can pass the detection threshold repeatedly and be counted multiple times. In principle, statistical pulse shape fluctuations can be smoothened out by low-pass filtering, but this may lead to unwanted pulse elongation.[22,24,25] In summary, larger values of PQ indicate better potential for achieving accurate counting and energy binning.

III.D. Stopping Power. Another material property that is important for an initial material selection is the stopping power of the scintillator. The stopping power of a scintillator is determined by its mass density and the effective atomic number. Ideally, the stopping power of a scintillator should be high enough to absorb all of the energy of the incident X-ray photon. Moreover, photoelectric absorption should be the main mechanism of interaction between the scintillator pixel and the incident X-ray photons. The higher the effective atomic number of a scintillator, the higher the probability of photoelectric absorption taking place. In order to take the stopping power into account a fourth FOM ($\rho Z_{eff}^{3.5}$) will be used. This product provides an indication of the stopping power and efficiency of photoelectric absorption. The larger this number, the better the stopping power and the larger the probability of photoelectric absorption. The effective attomic number (Z_{eff}) is defined as[48]

$$Z_{eff} = \sqrt[3.5]{\sum_i a_i Z_i^{3.5}} \quad (15)$$

It should be noted that the number $\rho Z_{eff}^{3.5}$ provides only an initial indication of the stopping power. The stopping power of a scintillator for X-rays in the diagnostic energy range (25 to 150 keV) will depend on the exact composition of the scintillator and the position of the K and L-edges.

III.E. Purpose and Scope of the Proposed FOMs. The four figures of merit described above are based on the emissive properties of a scintillator combined with the detection properties of a SiPM, and the density and composition of the scintillator. A candidate material should have a high pulse intensity, a short pulse duration, a high value of pulse quality, and a high value of $\rho Z_{eff}^{3.5}$. Such a material will efficiently absorb X-ray photons and convert them into a short and intense pulse of scintillation light, with a low probability of pulse pile-up and low statistical fluctuations of the detector output pulse amplitude and shape. It should be noted that other material properties,

https://doi.org/10.1021/acs.chemmater.4c03437
Chem. Mater. 2025, 37, 1716−1740

such as self-absorption, afterglow, radiation hardness, possibility to produce submillimeter pitch pixel arrays, and cost-effectiveness, are not taken into account in the FOMs formulated and discussed above. Such properties are of high importance for the applicability of a material in real-world PCDs. It should thus be noted that the FOMs presented here are only to be used for an initial selection of candidate materials.

IV. SCINTILLATOR OVERVIEW

An initial assessment of scintillators for their application in PCDs can be made by plotting the pulse quality over the pulse duration. However, not all scintillator and detector properties are readily available in the literature. For a first general material selection, the following assumptions are therefore made. First, the effective PDE ($\overline{\eta}_{det}$) is taken as 100%. Second, scintillator light yields are commonly determined and reported by using the 662 keV γ-photons of ^{137}Cs. This value is used to estimate the intensity of the scintillation pulse ($\overline{N}_{em}$) because data on nonproportionality or the light yield at clinically relevant X-ray energies is not always available. This results in $\overline{N}_{det} = \overline{N}_{em}$, which is taken to be equal to the light yield measured at 662 keV. Finally, not all scintillators show a single-exponential decay (cf. eq 8). For scintillators which show multiple decay components the average decay time constant is calculated according to

$$\overline{\tau}_{av} = \frac{\sum_{i=1}^{n} A_i \tau_{dec,i}^2}{\sum_{i=1}^{n} A_i \tau_{dec,i}} \quad (16)$$

Here, A_i represents the amplitude and $\tau_{dec,i}$ the decay time of the different decay components. The separate decay components can be found in the Supporting Information.

Based on the above three assumptions, data was collected from literature to asses the performance potential of different scintillators. The tabulated values of the energy resolution are defined as the fwhm of the photopeak at 662 keV. The tabulated values of the peak emission wavelength are defined as the peak wavelength of the most intense emission band. The tabulated values of the pulse duration are calculated based on a convolution of either the reported single-exponential decay time or the calculated average decay time, in combination with a SiPM recharge time constant of 7 ns. The tabulated values of the pulse quality are calculated based on the tabulated values of the light yield and pulse duration.

Solid-state scintillators can be subdivided into two general groups: extrinsically activated scintillators and intrinsic scintillators. Extrinsically activated scintillators can be divided into subgroups based on the used activator ion; typical activator ions are Ce^{3+}, Eu^{2+}, and Tl^{+}. In the past three decades, scintillation research has mainly focused on the development of Ce^{3+} and Eu^{2+}-doped compounds. An example is the development of $LaBr_3:Ce^{3+}$, which has a light yield of 76 ph/keV and decay time of 16 ns.[26] Alekhin et al. showed that codoping $LaBr_3:Ce^{3+}$ with Sr^{2+} improves the proportionality without affecting the light yield. This resulted in the current record energy resolution of 2% at 662 keV. Co-doping with Sr^{2+}, however, introduces several slow decay processes. Due to the additional weight that is given to slower decay components (eq 16), this results in an average decay time of 1.2 μs for $LaBr_3:Ce^{3+},Sr^{2+}$.[26,49] Other well-known Ce^{3+} based scintillators are $Lu_2SiO_5:Ce^{3+}$[50,51] and $(Lu,Y)_2SiO_5:Ce^{3+}$[52−54] which are used in positron emission tomography scanners due to their high density and relatively short decay time of around 40 ns.[55] Not all Ce^{3+}-doped scintillators show Ce^{3+} 5d → 4f emission exclusively. Some also show emission originating from the host matrix. An example of this is $Cs_2LiYCl_6:Ce^{3+}$, commonly used for the detection of neutrons.[56−58] The host emission introduces a slow component in the scintillation decay. The collected data on Ce^{3+}-doped scintillators are summarized in Table I.

Examples of Eu^{2+}-doped scintillators are SrI_2Eu^{2+}[59−61] and $CsBa_2I_5:Eu^{2+}$[62,63] with light yields of 90 and 97 photons/keV, respectively. The Eu^{2+} $4f^6 5d \rightarrow 4f^7$ transition, however, has a typical decay time between 500 and 1000 ns, making these scintillators 10−50 times slower than Ce^{3+}-doped scintillators. Additionally, Eu^{2+}-doped scintillators often suffer from self-absorption, due to a relatively small Stokes shift.[63−68] This is mainly a problem in applications where crystals larger than several millimeters are required. The collected data on Eu^{2+}-doped scintillators are summarized in Table II.

Two other divalent lanthanides that have been used as activator ions are Yb^{2+} and Sm^{2+}. Yb^{2+} is very similar to Eu^{2+} in spin-allowed decay time and emission wavelength. However, its decay always includes a slow millisecond component due to the spin-forbidden $4f^{13}5d \rightarrow 4f^{14}$ transition.[69] Sm^{2+}, on the other hand, emits in the near-infrared and has a decay time of approximately 2 μs.[70] It can be used as a codopant next to Eu^{2+} or Yb^{2+}, as their energy can efficiently be transferred to Sm^{2+}.[71−75] The collected data on Yb^{2+}, Eu^{2+}-Sm^{2+}, and Yb^{2+}-Sm^{2+} are summarized in Table III.

Another, less commonly used, lanthanide activator ion is Pr^{3+}.[76−81] It can show $4f^15d \rightarrow 4f^2$ emission in compounds where the energy of its $4f^15d$ state lies between that of the $4f^2[^1S_0]$ and $4f^2[^3P_2]$ states.[82] One of the main challenges of utilizing the fast $4f^15d \rightarrow 4f^2$ transition of Pr^{3+} is that it is located in the UV.[83] However, its shorter emission wavelength compared to the Ce^{3+} 5d → 4f emission also results in shorter decay times of typically 10 to 20 ns.[83] This is observed in $Lu_3Al_5O_{12}:Pr^{3+}$, for example.[84,85] The collected data on Pr^{3+}-doped scintillators is summarized in Table III.

The Tl^{+}-doped scintillators $CsI:Tl^{+}$[86] and $NaI:Tl^{+}$[87,88] have been studied extensively and are commercially available. The latter, discovered by Hofstadter in 1948,[89−91] is one of the first and most widely used scintillators to this day. The collected data on Tl^{+}-doped scintillators are summarized in Table III.

Intrinsic scintillators can be divided into four subgroups based on their emission: broad-band, near band gap excitonic, core−valence luminescence, and plastics. Each of these groups will be discussed in the next paragraphs, starting with the broad-band emitters.

Two well-known intrinsic broad-band scintillators are $Bi_4Ge_3O_{12}$ (BGO) and $PbWO_4$. BGO, due to its 300 ns decay time and density of 7.13 g/cm^3, is used in positron emission tomography detectors (PET).[92−94] $PbWO_4$ has a much lower light yield, but, due to is decay time of 30 ns and density of 8.28 g/cm^3, has been used in the Large Hadron Collider of CERN.[95,96] Intrinsic broad-band scintillators that have been explored more recently are the cesium hafmium-based halides,[97−100] cesium copper-based iodides,[101−103] and thallium-based halides.[104−107] These compounds typically show decay times on the order of 1 to 2 μs. The collected data on intrinsic broad-band emitting scintillators are summarized in Table IV.

The second subgroup is scintillators showing near band gap excitonic emission. Examples of materials in this subgroup are the inorganic perovskites,[108−112] and the hybrid organic−inorganic perovskites and perovskite-related compounds.[113−121]

https://doi.org/10.1021/acs.chemmater.4c03437
Chem. Mater. 2025, 37, 1716−1740

Table I. Light Yield (photons/keV) Measured at 662 keV, fwhm Energy Resolution (E%) Measured at 662 keV, Decay Time Constant (τ_{dec} (ns)), Peak Emission Wavelength (λ_{em} (nm)), Mass Density (g/cm^3), $\rho Z_{eff}^{3.5}$ Calculated Based on Tabulated Compound Composition and Mass Density, Pulse Duration Calculated Assuming a SiPM Recharge Time Constant of 7 ns (t_{fwhm} (ns)), and Pulse Quality Calculated Based on Tabulated Values of the Light Yield and Pulse Duration (PQ (photons/keV/ns)$^{1/2}$) of Ce^{3+}-Doped Scintillators

Compound	Light yield (Ph/keV)	E% @662 keV	τ_{dec} (ns)	λ_{em} (nm)	Density (g/cm^3)	$\rho Z_{eff}^{3.5}$ (10^6)	t_{fwhm} (ns)	PQ (Ph/keV/ns)$^{1/2}$	ref
CeF_3	4	20%	27	340	6.16	6.41	36.3	0.332	190
$LaCl_3$	46	3.1%	169[a]	337	3.86	2.68	143	0.566	191−193
$LuCl_3$	5.4	11.4%	5,572[a]	374/400	4	7.53	3,920	0.037	192,194
K_2LaCl_5	29	5.1%	68	380	2.89	1.47	68.6	0.650	195
K_2CeCl_5	30	5.8%	71	370	2.95	1.60	70.9	0.650	196,197
KGd_2Cl_7	30	10%	179[a]	400	3.56	3.94	151	0.446	198
$CsSrCl_3$	8.6	7.2%	603[a]	360/385	2.96	1.77	453	0.138	199
Cs_3LaCl_6	16	8.6%	1,026[a]	380/407	3.36	3.28	750	0.146	200
$CsCe_2Cl_7$	28	5.5%	50	410	3.6	3.19	54.8	0.715	201
Cs_3CeCl_6	19	8.4%	265[a]	385	3.4	3.19	213	0.299	202
Cs_3GdCl_6	24	4.5%	2,008[a]	380/405	3.56	3.83	1,437	0.131	203
Tl_2LaCl_5	70	3.4%	895[a]	383	5.2	15.44	658	0.326	204,205
Tl_2GdCl_5	53	5%	1,330[a]	389	5.1	15.70	963	0.235	206
$Rb_2LiCeCl_6$	23	7.9%	239[a]	370	3.1	1.55	194	0.344	207
$Rb_2LiGdCl_6$	18	6.8%	3,490[a]	375/420	3.23	2.28	2,471	0.087	208
Cs_2LiYCl_6	22	4.5%	6,000	376/404	3.31	2.10	4,219	0.720	209,210
$Cs_2LiLaCl_6$	35	3.4%	445[a]	340/420	3.3	2.78	341	0.320	211
$Cs_2LiCeCl_6$	22	5.5%	2,263[a]	410	3.41	2.95	1,615	0.117	212
$Cs_2LiGdCl_6$	20	5%	7,706[a]	380/405	3.67	3.78	5,404	0.061	213
$Cs_2NaLaCl_6$	26	4.4%	1,513[a]	373/405	3.26	2.68	1,091	0.156	200
$Cs_2NaCeCl_6$	20	8.3%	2,696[a]	410	3.25	2.74	1,917	0.102	214
$Cs_2NaGdCl_6$	27	4%	3,030[a]	375/403	3.52	3.54	2,151	0.112	203,215
Tl_2LiYCl_6	25	4%	777[a]	435	4.5	12.50	575	0.208	216
$Tl_2LiGdCl_6$	58	4.6%	868[a]	376/382	n.r.	n.r.	639	0.301	217
$Tl_2LiLuCl_6$	27	5.6%	1,373[a]	428	5.06	15.66	993	0.165	218
$BaBr_2$	10	9.8%	1,935[a]	375/410	4.84	3.60	1,386	0.086	219
$LaBr_3$	76	2.7%	16	358	5.29	3.56	26.5	1.515	26,220,221
$LaBr_3$:Ce,Sr	78	2%	1,209[a]	356/382	5.29	3.56	878	0.298	26,49,162
$LaBr_{2.25}I_{0.75}$	45	4.1%	117[a]	400/434	5.47	4.19	149	0.548	222
$LaBr_{1.5}I_{1.5}$	58	14.6%	28	472/500	5.51	4.98	37.1	1.249	222
$LaBr_{0.75}I_{2.25}$	22	35.9%	12	460/510	5.6	5.72	22.6	0.986	222
$CeBr_3$	60	3.6%	17	370	5.2	3.68	27.5	1.477	223,224
$CeBr_3$:Sr	55	3%	65[a]	381	5.2	3.68	66.3	0.911	225−227
$PrBr_3$:20%Ce	21	6.9%	7.9	365/395	5.33	3.69	18.2	1.075	155
$PrBr_3$:5%Ce	16	5.5%	5.6	365/395	5.33	3.69	15.3	1.022	155
$GdBr_3$	44	10%	698[a]	419	4.6	4.53	520	0.291	228
$LuBr_3$	32	6%	3,433[a]	408/448	5.17	7.34	2,430	0.115	192,194
K_2LaBr_5	40	5%	50	359/391	3.9	1.88	54.8	0.854	229
Rb_2CeBr_5	34	6.9%	56.1	390	4.26	2.17	59.5	0.756	230
$RbGd_2Br_7$	54	3.8%	60	425	4.7	4.06	62.5	0.929	231
Cs_3LaBr_6	32	4.9%	2,042[a]	395/425	4.55	3.61	1,461	0.149	200,232
$CsCe_2Br_7$	33	7%	1,222[a]	450	4	2.97	888	0.200	233
Cs_3GdBr_6	47	4%	1,289[a]	396/417	4.14	3.92	935	0.224	203
Tl_2LaBr_5	43	5%	25	375/315	5.9	14.02	34.6	1.115	234
Rb_2LiYBr_6	23	4.7%	1,199[a]	385/420	3.82	1.06	871	0.162	235
$Rb_2LiLaBr_6$	33	4.8%	978[a]	363/387	n.r.	n.r.	716	0.215	236
$Rb_2LiCeBr_6$	33	6.3%	155[a]	373	4.6	2.21	133	0.497	213
Cs_2LiYBr_6	23	7%	2,492[a]	389	4.15	2.38	1,775	0.115	210,237
$Cs_2LiLaBr_6$	60	2.9%	540[a]	380/430	4.2	3.03	408	0.383	238−240
$Cs_2LiCeBr_6$	28	7.4%	3,289[a]	400/418	4.18	3.08	2,330	0.110	241
$Cs_2LiGdBr_6$	30	7.1%	3,477[a]	392/400	4.41	3.90	2,462	0.111	242
Cs_2NaYBr_6	9.5	6.3%	2,543[a]	385/420	3.94	2.22	1,810	0.072	243
$Cs_2NaYBr_3I_3$	43	3.3%	1,795[a]	425/460	n.r.	n.r.	1,288	0.183	244
$Cs_2NaLaBr_6$	46	3.9%	3,535[a]	382/414	3.93	2.79	2,501	0.136	200,243
$Cs_2NaLaBr_3I_3$	58	2.9%	1,089[a]	430	n.r.	n.r.	794	0.270	244

https://doi.org/10.1021/acs.chemmater.4c03437
Chem. Mater. 2025, 37, 1716−1740

Table I. continued

Compound	Light yield (Ph/keV)	E% @662 keV	τ_{dec} (ns)	λ_{em} (nm)	Density (g/cm^3)	$\rho Z_{eff}^{3.5}$ (10^6)	t_{fwhm} (ns)	PQ (Ph/keV/ns)$^{1/2}$	ref
$Cs_2NaCeBr_6$	25	6.7%	352[a]	377	4.25	3.08	275	0.301	245
$Cs_2NaGdBr_6$	48	3.3%	396[a]	393/422	4.18	3.63	306	0.396	203,246
Cs_2 $NaLuBr_6$	10	5.5%	280[a]	389/422	4.42	4.58	223	0.217	243
$Tl_2LiGdBr_6$	17	17%	91[a]	422	5.3	12.12	86.2	0.449	247
SrI_2:Ce,Na	16	6.4%	426[a]	404/434	4.59	4.10	327	0.221	61
YI_3	99	9.3%	45	532	4.62	4.38	50.8	1.395	248
GdI_3	44	4.3%	45	532	5.22	7.20	50.8	0.930	248,249
LuI_3	98	3.3%	85[a]	472	5.6	9.48	81.5	1.097	250−252
K_2LaI_5	55	4.5%	24	401/439	4.4	4.57	33.7	1.277	229
$Cs_3Lu_2I_9$	22	9%	446[a]	429/471	4.78	7.04	342	0.258	232
Cs_2NaLaI_6	26	4.4%	1,513[a]	420/458	4.17	4.73	1,091	0.156	200
$YAlO_3$	15	4.4%	35[a]	347	5.35	1.08	42.9	0.609	253−255
$Y_3Al_5O_{12}$	14	12%	70	550	4.55	0.77	70.2	0.447	256
$LuAlO_3$	11	9.3%	43[a]	365	8.34	17.62	49.3	0.481	257
$Lu_3Al_5O_{12}$	12	12%	50	500/560	6.7	12.46	54.8	0.478	258
Y_2SiO_5	24	9.4%	42	420	4.45	1.03	48.5	0.703	259,260
Gd_2SiO_5	12	7%	336[a]	430	6.71	10.48	285	0.209	259,261
$Gd_2Si_2O_7$	30	6%	46	372/394	5.5	7.53	51.6	0.762	262
Lu_2SiO_5	27	7.9%	40	420	7.4	17.06	46.9	0.759	50
Lu_2SiO_5:Ce,Ca	38	7.7%	36.7	420	7.4	17.06	44.3	0.936	51
$Lu_2Si_2O_7$	26	10%	38	378	6.2	12.64	45.3	0.757	263,264
$(Lu_{0.9}Y_{0.1})_2SiO_5$	27	8%	36	425	7.1	15.41	43.7	0.786	52−54
$K_2Lu(PO_4)_2$	26	17%	1,074[a]	390	3.90	4.67	784	0.184	265

[a]Decay consists of multiple components, tabulated value was calculated using eq 16. The amplitudes and decay times of the different components can be found in Table S1.

Specifically, two-dimensional perovskites have shown to be promising scintillators due to their stable room-temperature near band gap excitonic emission.[122,123] Their nanosecond decay time makes them very interesting for use in a PCD. This possibility has been explored with benzylamonium lead bromide ($(BZA)_2PbBr_4$).[124] Xia et al. have demonstrated that the decay time of 2D hybrid organic−inorganic perovskites can be reduced even further by engineering the dielectric constant of the organic molecule.[125,126] A downside to these materials, however, is their low density of approximately 2.5 g/cm^3. The collected data on the near band gap exciton scintillators are summarized in Table IV.

The third subgroup consists of scintillators showing core−valence luminescence. Such an emission originates from the recombination of an electron in the valence band with a hole in the highest core band. This is referred to as core−valence luminescence (CVL), cross luminescence, or auger-free luminescence.[127] It can only take place when the condition formulated in eq 17 is satisfied.[128]

$$E_{CV} + \Delta E_V < E_g \tag{17}$$

Here, E_{CV} represents the energy gap between the highest core band and the bottom of the valence band, ΔE_V is the width of the valence band, and E_g is the band gap. This condition is satisfied in some fluorides, chlorides, and bromides containing Ba^{2+}, Cs^+, Rb^+, and K^+.[129] One of the first compounds in which CVL was discovered is BaF_2.[130] The emission spectrum of BaF_2 contains three CVL bands, at 183, 196, and 220 nm, in addition to the self-trapped exciton band at 310 nm.[131] The CVL bands have a decay time of 0.8 ns, while the self-trapped exciton band has a decay time of 600 ns. The short decay time of the CVL emission makes these materials potential candidates for use in a PCD. One of the main problems, however, is the presence of STE or other emissions with longer decay times. The self-trapped exciton emission of BaF_2 can be suppressed by doping BaF_2 with, for example, La^{3+},[132,133] Cd^{3+},[132,133] Y^{3+},[134,135] and Sc^{3+}.[136] The CVL bands of fluoride-based compounds are approximately between 140 and 230 nm. The emission wavelength shifts to longer wavelengths in chloride- and bromide-based compounds. Examples of chloride-based compounds that show CVL emission are the families of Cs−Mg−Cl and Cs−Zn−Cl compounds.[137−139] An advantage of these compounds is the absence of slow decay components at room temperature. The collected data on fluoride- and chloride-based compounds that show CVL emission are summarized in Table V. Bromide-based compounds like CsBr, $CsCaBr_3$, and $CsSrBr_3$ are not considered due to their low CVL intensity.[127,129,140,141]

The last subgroup consists of plastic scintillators. These materials are often used for the detection of neutrons.[142−144] Plastic scintillators typically have a density of about 1 g/cm^3 and contain low Z atoms, like carbon and hydrogen, which makes these materials less suitable for the detection of high-energy γ-photons. High-Z dopants can be added to a plastic scintillator to increase its absorption.[145−147] The collected data on plastic scintillators are summarized in Table VI.

V. SCINTILLATOR ASSESSMENT

Using the FOMs and collected data discussed above, an assessment of the suitability of different scintillators for their use in indirect PCDs is made. To this end, the pulse duration is calculated as the fwhm of the average detector output pulse (eq 12), assuming a SiPM recharge time of 7 ns. The result is plotted versus the pulse quality (eq 14) in Figure 3. For reference, the pulse duration of CdTe (14 ns fwhm) is indicated by the red vertical line, providing a benchmark for the pulse duration requirements of an indirect PCD.

https://doi.org/10.1021/acs.chemmater.4c03437
Chem. Mater. 2025, 37, 1716−1740

Table II. Light Yield (photons/keV) Measured at 662 keV, fwhm Energy Resolution (E%) Measured at 662 keV, Decay Time Constant (τ_{dec} (ns)), Peak Emission Wavelength (λ_{em} (nm)), Mass Density (g/cm^3), $\rho Z_{eff}^{3.5}$ Calculated Based on Tabulated Compound Composition and Mass Density, Pulse Duration Calculated Assuming a SiPM Recharge Time Constant of 7 ns (t_{FWHM} (ns)), and Pulse Quality Calculated Based on Tabulated Values of the Light Yield and Pulse Duration (PQ (photons/keV/ns)$^{1/2}$) of Eu^{2+}-Doped Scintillators

Compound	Light yield (Ph/keV)	E% @662 keV	τ_{dec} (ns)	λ_{em} (nm)	Density (g/cm^3)	$\rho Z_{eff}^{3.5}$ (10^6)	t_{fwhm} (ns)	PQ (Ph/keV/ns)$^{1/2}$	ref
CaF_2	24	6.7%	900	440	3.18	0.06	662	0.190	266,267
BaFI	55	8.5%	500	450	5.45	6.10	380	0.380	268,269
$BaCl_2$	52	3.5%	604[a]	402	3.89	3.40	454	0.338	219,270
BaClBr	52	3.55%	500	425	4.5	3.59	380	0.370	268,269
BaClI	54	9%	500	425	4.5	4.79	380	0.377	268,269
$CsCaCl_3$	18	8.9%	5,050	450	3	1.80	3,558	0.071	271
$CsSrCl_3$	33	11.5%	2,700	448	2.96	1.77	1,920	0.132	272
$CsSrClBr_2$	35	3.6%	2,100	462	3.98	2.25	1,502	0.153	273
$CaBr_2$	36	8.9%	2,500	448	3.35	0.70	1,780	0.142	274
$BaBr_2$	49	6%	672[a]	408	4.78	3.56	501	0.315	219,275
BaBrI	91	3.4%	453[a]	413	5.18	5.09	347	0.512	276,277
$LiSr_2Br_5$	32	6.1%	1,418	407/476	3.76	1.04	1,024	0.177	278
KSr_2Br5	75	3.5%	1,013[a]	427	3.98	1.05	741	0.318	279
$RbCaBr_3$	43	4.0%	2,800	436	3.46	0.84	1,990	0.147	280
Rb_4CaBr_6	71	6.9%	5,360[a]	457	3.46	0.92	3,774	0.137	280
$RbSr_2Br_5$	64	4%	780	429	4.18	1.18	577	0.335	281
$CsCaBr_3$	28	9.3%	5,270	447	3.68	2.02	3,710	0.087	282
$CsCaBrI_2$	51	3.9%	3,500	445	3.59	3.26	2,478	0.145	273
$CsCaBr_{0.8}I_{2.2}$	40	5.2%	2,290	450	4.06	3.81	1,633	0.156	283
$CsSrBr_3$	40	4.9%	2,300	440	3.76	2.08	1,640	0.157	284
$CsSrBrI_2$	65	3.4%	1,800	455	4	3.53	1,292	0.225	273
LiI	15	7.5%	1,200	475	4.08	4.19	872	0.131	285,286
CaI_2	90	5.2%	790	470	3.96	3.73	584	0.392	287,288
SrI_2	90	2.6%	1,200	453	4.6	4.10	872	0.321	59−61
SrI_2:Eu,Zr	95	2.5%	1,030	436	4.6	4.10	753	0.355	163
BaI_2	38	5.6%	513	426	5.15	6.00	389	0.312	275
$LiCa_2I_5$	90	5.6%	1,416	472	4	3.83	1,023	0.297	278
$LiSrI_3$	35	5.2%	510	420/460	n.r.	n.r.	387	0.301	289
$LiSr_2I_5$	60	3.5%	1,331	497	n.r.	n.r.	964	0.249	278
$KCaI_3$	72	3%	1,060	466	3.81	3.44	774	0.305	290
$KCaI_3$:Eu,Zr	72	2.5%	1,313[a]	450	3.81	3.44	951	0.275	164
$KCa_{0.8}Sr_{0.2}I_3$	73	2.8%	1,258	475	3.81	3.42	913	0.283	64,291
KSr_2I_5	94	2.4%	2,531[a]	445	4.39	3.87	1,802	0.228	292
KBa_2I_5	90	2.4%	910	444	4.52	5.00	669	0.367	293
K_2BaI_4	63	2.9%	720	448	4.05	4.11	535	0.343	293
$RbSrI_3$	24	2.8%	1,030	462	4.1	3.47	753	0.323	294
$RbSr_2I_5$	90	3%	890	445	4.55	3.93	654	0.372	281
$CsCaI_3$	38	8%	1,720	450	4.06	4.24	1,236	0.176	271
Cs_4CaI_6	51	3.6%	1,990	459	3.99	4.44	1,425	0.191	295,296
$CsSrI_3$	73	3.9%	3,300	452	4.25	4.29	2,338	0.177	66
Cs_4SrI_6	62	3.5%	1,430	462	4.03	4.41	1,033	0.246	295,296
$CsBa_2I_5$	97	2.3%	350	430	5	5.82	273	0.595	62,63
$TlSr_2I_5$	70	4.2%	2,465[a]	463	5.3	9.01	1,756	0.200	297
Cs_3KCaI_6	62	3.9%	1,860	472	3.94	4.20	1,334	0.216	295
Cs_3KSrI_6	29	5%	1,780	459	3.85	4.03	1,277	0.151	295
Cs_3RbCaI_6	38	4.5%	1,250	467	3.96	4.14	907	0.205	295
$Cs_{3.5}Rb_{0.5}SrI_6$	75	3.3%	1,340	466	4.03	4.28	970	0.278	295
Cs_3RbSrI_6	31	5.1%	1,220	462	3.95	4.14	886	0.187	295

[a]Decay consists of multiple components, tabulated value was calculated using eq 16. The amplitudes and decay times of the different components can be found in Table S2.

Figure 3 shows that most data points from Eu^{2+}, Yb^{2+}, Sm^{2+}, Tl$^+$ and broad-band emission based scintillators have pulse durations longer than 100 ns fwhm. This results in pulse qualities typically below 0.400 (photons/keV/ns)$^{1/2}$, even though light yields of up to 90 photons/keV have been reported for compounds like SrI_2:Eu^{2+}.[59,60] The pulse duration of Ce^{3+}-doped scintillators ranges from tens of nanoseconds to tens of microseconds; the average decay time of Ce^{3+} strongly depends

https://doi.org/10.1021/acs.chemmater.4c03437
Chem. Mater. 2025, 37, 1716−1740

Table III. Light Yield (photons/keV) Measured at 662 keV, fwhm Energy Resolution (E%) Measured at 662 keV, Decay Time Constant (τ_{dec} (ns)), Peak Emission Wavelength (λ_{em} (nm)), Mass Density (g/cm^3), $\rho Z_{eff}^{3.5}$ Calculated Based on Tabulated Compound Composition and Mass Density, Pulse Duration Calculated Assuming a SiPM Recharge Time Constant of 7 ns (t_{FWHM} (ns)), and Pulse Quality Calculated Based on Tabulated Values of the Light Yield and Pulse Duration (PQ (photons/keV/ns)$^{1/2}$) of Scintillators with Activator Ions Other than Ce^{3+} or Eu^{2+}

Compound	Light yield (Ph/keV)	E% @662 keV	τ_{dec} (ns)	λ_{em} (nm)	Density (g/cm^3)	$\rho Z_{eff}^{3.5}$ (10^6)	t_{fwhm} (ns)	PQ (Ph/keV/ns)$^{1/2}$	ref
$LaBr_3$:Pr	60	3.2%	11,000	492−682	5.29	3.56	7,695	0.088	298
$Lu_3Al_5O_{12}$:Pr	19	4.6%	20.1	325	6.7	12.46	30.3	0.791	84,85
$(Lu,Y)_3Al_5O_{12}$:Pr	33	4.4%	1,080[a]	325	6.2	14.04	788	0.205	299−301
$(Lu,Y)_3Al_5O_{12}$:Pr,Li	25	4.1%	1,180[a]	325	6.2	14.04	858	0.171	301
SrI_2:Eu,Sm	42	10.5%	1,500	740	4.59	4.10	1,082	0.197	71
$CsBa_2I_5$:Eu,Sm	45	3.2%	2,077[a]	755	5	5.82	1,485	0.174	72
Cs_4EuI_6:Sm	16	7.5%	3,500	850	4.25	5.24	2,478	0.082	73
$CsYbI_3$:Sm	30	7%	2,300	800	4.76	7.44	1,640	0.135	74
NaI:Tl	38	5.4%	250	415	3.67	3.37	202	0.433	86−88
NaI:Tl,Ca	26	5.3%	380[a]	420	3.67	3.37	295	0.297	302
NaI:Tl,Sr	34	5.4%	327[a]	420	3.67	3.37	257	0.363	302
NaI:Tl,Ca,Eu	52	4.9%	1,000	450	3.67	3.37	732	0.266	303,304
CsI:Tl	54	4.8%	1,000	550	4.51	5.23	732	0.272	86,87,305
SrI_2:Yb	56	4.35%	610	414	4.6	4.10	458	0.350	306
$RbSrI_3$:Yb	24	4.9%	795	457	4.1	3.47	588	0.202	294
$CsBa_2I_5$:Yb	54	5.7%	870	414	5	5.82	640	0.290	306

[a]Decay consists of multiple components, tabulated value was calculated using eq 16. The amplitudes and decay times of the different components can be found in Table S3.

on the host matrix. This can be explained by inefficient or slow transfer of charge carriers toward Ce^{3+} and the presence of host-related emissions next to the intrinsic 5d → 4f emission of Ce^{3+}. There are several Ce^{3+}-based scintillators that approach the pulse duration of CdTe, i.e., $LaBr_3$:Ce^{3+} and $CeBr_3$.

The situation of Pr^{3+}-doped scintillators is very similar to that of Ce^{3+}-doped scintillators. The average decay time of Pr^{3+} depends strongly on the host matrix, i.e. the occurrence of efficient 5d → 4f emission. For example, $Lu_3Al_5O_{12}$:Pr^{3+} shows efficient 5d → 4f emission and has a pulse duration of 30.3 ns fwhm. $LaBr_3$:Pr^{3+}, on the other hand, shows only 4f → 4f emission and has a pulse duration of 7.6 μs. The shorter emission wavelength of Pr^{3+} decreases its intrinsic 5d → 4f decay time compared to that of Ce^{3+}. The main challenge for Pr^{3+} however is the efficient detection of its UV emission.

The shortest pulse durations are achieved by a scintillator based on CVL emission, near-bandgap exciton emission, and plastics, with some materials showing pulse durations shorter than CdTe. However, these different types of scintillators each have their respective challenges. For CVL emitters, for example, these include the presence of slow decay components or the low light yield of the CVL emission.

For near band gap exciton emitters, self-absorption is a big challenge.[114,148,149] Self-absorption refers to the reabsorption of emitted scintillation photons within the scintillation crystal. It is a direct result of spectral overlap between the excitation and emission spectra of the scintillator; the energy difference between these two is referred to as the Stokes shift. Self-absorption can decrease the observed light yield due to a higher probability of nonradiative losses. In case the probability of re-emission after self-absorption is very high, i.e., close to 1, the influence on the observed light yield may remain small, but the observed scintillation decay may still be elongated, especially in large crystals.[150,151] Self-absorption is also a problem in Eu^{2+}-doped scintillators in which it has been studied extensively.[63−68,152,153] It has been demonstrated that the self-absorption in Eu^{2+}-doped scintillators can be mitigated by codoping these materials with Sm^{2+}.[71,73,75] The role and impact of self-absorption in near band gap exciton emitters is discussed elaborately by Yan et al.[149]

Plastic scintillators show very promising values for their pulse quality and pulse duration. However, one of the main problems with these materials is their low density, typically about 1 g/cm^3, and low stopping power. Plastic scintillators mostly contain low-Z elements like hydrogen, carbon, nitrogen, and oxygen. Because their exact composition is not always known, it was not possible to calculate the value of $\rho Z_{eff}^{3.5}$ for these materials. The low stopping power and effective atomic number does not only result in the need for very large pixels to absorb the energy of incident X-ray photons but also makes Compton scattering the dominant interaction mechanism. Scattered X-ray photons can be detected in neighboring pixels, resulting in multiple detected events for one incident X-ray photon.

Figure 4 shows the decay time versus the pulse duration for the collected data points. The red vertical line indicates the 7 ns recharge time of the SiPM used to calculate the pulse duration. Three different regimes can be identified in this plot. When the decay time is significantly shorter than the SiPM recharge time, the pulse duration is determined almost entirely by the recharge time ($t_{fwhm}(\tau_{rech})$) and, therefore, the pulse duration is of a given, finite length, no matter how fast the scintillator emits. This regime lies on the left-hand side of the left-most black vertical line in Figure 4. There are no data points in this regime. On the other hand, when the decay time is significantly longer than the recharge time, the pulse duration is mainly determined by the decay time ($t_{fwhm}(\tau_{dec})$). This regime lies on the right-hand side of the rightmost black vertical line. In these extreme cases, the pulse duration can be estimated based on a single exponential decay, as indicated by the horizontal and diagonal dashed asymptotes, respectively. In the middle regime ($t_{fwhm}(\tau_{dec}, \tau_{rech})$), where τ_{rech} and τ_{dec} are of comparable magnitudes, the

https://doi.org/10.1021/acs.chemmater.4c03437
Chem. Mater. 2025, 37, 1716−1740

Table IV. Light Yield (photons/keV) Measured at 662 keV, fwhm Energy Resolution (E%) Measured at 662 keV, Decay Time Constant (τ_{dec} (ns)), Peak Emission Wavelength (λ_{em} (nm)), Mass Density (g/cm^3), $\rho Z_{eff}^{3.5}$ Calculated Based on Tabulated Compound Composition and Mass Density, Pulse Duration Calculated Assuming an SiPM Recharge Time Constant of 7 ns (t_{FWHM} (ns)), and Pulse Quality Calculated Based on Tabulated Values of the Light Yield and Pulse Duration (PQ (photons/keV/ns)$^{1/2}$) of Undoped Scintillators

Compound	Light yield (Ph/keV)	E% @662 keV	τ_{dec} (ns)	λ_{em} (nm)	Density (g/cm^3)	$\rho Z_{eff}^{3.5}$ (10^6)	t_{fwhm} (ns)	PQ (Ph/keV/ns)$^{1/2}$	ref
$BaCl_2$	1.7	17.4%	980	300/410	3.89	3.40	718	0.049	307
$(EDBE)PbCl_4$	9	30%	7.9	520	2.19	4.57	18.2	0.704	121
Cs_2HfCl_6	54	3.3%	2,200	375/435	3.86	5.27	1,751	0.185	97,308
Cs_2ZrCl_6	33	4.5%	1,500	440/479	3.36	2.18	1,082	0.177	97,308
$TlMgCl_3$	30	3.7%	413[a]	409	4.43	12.96	318	0.310	104
$TlCaCl_3$	30	5%	622[a]	425	3.77	10.54	466	0.256	105
Tl_2HfCl_6	27	3.7%	1,063[a]	460	5.1	16.10	776	0.590	106,107
Tl_2ZrCl_6	35	3.4%	2,292[a]	460	4.5	12.61	1,635	0.146	106,107
$BaBr_2$	19	5.4%	2,200	425	4.78	3.56	1,571	0.111	307
$(BM)_2PbBr_4$[b]	3.2	19.53%	0.95	440	2.05	3.00	7.7	0.643	125
$(BZA)_2PbBr_4$[b]	3.7	8%	4.2	440	2.3	3.45	13.4	0.526	124
$(PEA)_2PbBr_4$[b]	11	39%	35	440	2.36	3.42	42.9	0.506	120,309
$TlCaBr_3$	41	6.2%	2,328[a]	470	4.69	10.07	1,660	0.158	310
$TlSr_2Br_5$	37	4.6%	1,470[a]	441	5.03	7.35	1,061	0.188	311
CaI_2	107	3.2%	834	410	3.96	3.73	616	0.417	287,288,312
$RbSrI_3$	8	7.6%	918[a]	447	4.1	3.47	674	0.109	294
$CsCu_2I_3$	16	7.8%	110	560	5.01	4.64	100	0.399	101,102
$Cs_3Cu_2I_5$	29	3.4%	965[a]	450	4.51	4.65	707	0.202	103
Cs_2HfI_6	64	4.2%	2,500	700	5.12	7.30	1,780	0.190	99,100
$Cs_3Lu_2I_9$	6.6	19.2%	770	390/608	4.82	7.10	570	0.108	232
$TlCaI_3$	42	6.2%	1,105[a]	460/533	4.73	10.53	805	0.229	104
$TlSr_2I_5$	31	8.5%	2,372[a]	463	5.3	9.01	1,691	0.135	297
Sc_2O_3	19	16.7%	290[a]	330	3.83	0.11	231	0.288	313
$CaWO_4$	15	6.6%	8,722[a]	425	6.1	13.61	6,113	0.051	314−316
$CdWO_4$	15	9.1%	15,000[a]	480	7.9	15.95	10,480	0.038	266,317
$PbWO_4$	0.3	n.r.	26[a]	420	8.28	30.49	15.8	0.138	95,318,319
$Bi_4Ge_3O_{12}$	7.6	9.05%	300	485	7.13	25.16	238	0.179	253,261,320

[a]Decay consists of multiple components, tabulated value was calculated using eq 16. The amplitudes and decay times of the different components can be found in Table S4. [b]Compounds show near-bandgap exciton emission.

pulse duration is determined by both of them. This is the region of Figure 4 in which interesting data points are found.

VI. SCINTILLATOR ENGINEERING

In addition to selecting scintillators for application in an indirect PCD it is also possible to optimize one. There are various ways in which this can be achieved, for example T_{50} engineering or codoping. More recently it has also been suggested that the properties of hybrid organic−inorganic perovskites can be tailored by specifically changing the dielectric constant of the organic layer.[125,126]

VI.A. T_{50} Engineering. The performance of a scintillator in an indirect PCD can sometimes be improved by quenching its emission, thereby making its decay faster. This strategy shortens the pulse duration and allows the scintillator to handle a higher count rate. Even though quenching causes a decrease in light yield, from a theoretical perspective, the amplitude of the scintillation pulse is independent of temperature everywhere along the quenching curve. The same applies to the pulse quality, as long as the decay time is much longer than the recharge time of the SiPM (in other words, in the regime in which the pulse duration is mainly determined by τ_{dec}). For illustrative purposes, the effect on the decay time and pulse quality of quenching a scintillator's emission is modeled assuming a hypothetical scintillator with a light yield of 140,000 ph/MeV and a decay time τ_{dec} = 140 ns at zero kelvin. It is assumed that the quenching curve can be described using a single-barrier Arrhenius equation:[154,155]

$$I(T) = \frac{I(0)}{1 + \frac{\Gamma_0}{\Gamma_\upsilon}\cdot e^{-\Delta E/k_B T}} \tag{18}$$

$$\tau_{dec}(T) = \frac{\tau_\upsilon}{1 + \frac{\Gamma_0}{\Gamma_\upsilon}\cdot e^{-\Delta E/k_B T}} = \frac{I(T)}{I(0)}\tau_\upsilon \tag{19}$$

where $I(T)$ represents the luminescence intensity at the absolute temperature T, $I(0)$ the luminescence intensity at $T = 0$ K, Γ_0 the attempt rate for thermal quenching, Γ_υ the radiative decay rate, k_B the Boltzmann constant, and ΔE the energy barrier. In eq 19, $\tau_{dec}(T)$ represents the decay time at the absolute temperature T and τ_υ is the decay time at $T = 0$.

Based on eqs 18 and 19, the change in light yield and decay time can be calculated along the quenching curve; when the light yield is halved, the decay time is also halved. This allows for the calculation of multiple points along the quenching curve. Based on the resulting values of the light yield and decay time, the pulse duration and pulse quality are calculated. Additionally, the light yield and decay time are used as input for the experimentally

https://doi.org/10.1021/acs.chemmater.4c03437
Chem. Mater. 2025, 37, 1716−1740

Table V. Light Yield (photons/keV) Measured at 662 keV, fwhm Energy Resolution (E%) Measured at 662 keV, Decay Time Constant (τ_{dec} (ns)), Peak Emission Wavelength (λ_{em} (nm)), Mass Density (g/cm^3), $\rho Z_{eff}^{3.5}$ Calculated Based on Tabulated Compound Composition and Mass Density, Pulse Duration Calculated Assuming an SiPM Recharge Time Constant of 7 ns (t_{FWHM} (ns)), and Pulse Quality Calculated Based on Tabulated Values of the Light Yield and Pulse Duration (PQ (photons/keV/ns)$^{1/2}$) of Scintillators Showing Core−Valence Luminescence

Compound	Light yield (Ph/keV)	E% @662 keV	τ_{dec} (ns)	λ_{em} (nm)	Density (g/cm^3)	$\rho Z_{eff}^{3.5}$ (10^6)	t_{fwhm} (ns)	PQ (Ph/keV/ns)$^{1/2}$	ref
RbF	1.7	n.r.	1.3	203/234	3.6	0.90	8.4	0.451	321
BaF_2	12	11%	630[a]	220/310	4.88	4.97	472	0.159	322−324
CsF	1.9	20%	2	390	4.64	4.98	9.8	0.441	325
$KMgF_3$	1.4	n.r.	1.3	140/170	3.2	0.04	8.4	0.409	127,321,326
$KCaF_3$	1.4	n.r.	2	165/200	3	0.06	9.8	0.379	127,321
KYF_4	1	n.r.	1.9	170	3.6	0.59	9.6	0.323	127,321
K_2YF_5	0.3	n.r.	1.3	170	3.6	0.48	8.4	0.189	321
$KLuF_4$	0.2	n.r.	1.3	163/185	5.2	9.36	8.4	0.143	127,129,321
KLu_2F_7	0.3	n.r.	2	165	7.5	14.98	9.8	0.166	321
$CsMgCl_3$	1.1	n.r.	2.36	350	3.23	2.04	10.5	0.326	127
$CsMgCl_3$:Zn	3.4	16.7	2.17	300	3.23	2.04	10.0	0.581	139
Cs_2MgCl_4	2.2	22	2.04	300	2.95	2.26	9.8	0.473	138,139
Cs_2MgCl_4:Zn	2.4	19.2	1.91	300	2.95	2.26	9.6	0.504	139
Cs_3MgCl_5	1.3	33.7	1.46	300	3.15	2.60	8.7	0.392	138,139
Cs_3MgCl_5:Zn	2.1	22.8	1.25	300	3.15	2.60	8.3	0.514	139
$CsCaCl_3$	1.4	n.r.	2	250/305	2.9	1.74	9.8	0.379	321,327
Cs_2ZnCl_4	2	22%	1.66	285/379	3.35	2.41	9.2	0.464	137
Cs_3ZnCl_5	1.4	25%	0.82	240/289	3.44	2.71	7.3	0.449	137
$CsSrCl_3$	0.9	n.r.	2.07	248	2.87	1.72	10.0	0.299	127,328
Cs_2BaCl_4	1.4	n.r.	1.68	400	3.76	3.53	9.2	0.386	127
Cs_2LiYCl_6	22	11%	6,599[a]	325	3.31	2.10	4,634	0.070	209,210

[a]Decay consists of multiple components, tabulated value was calculated using eq 16. The amplitudes and decay times of the different components can be found in Table S5.

Table VI. Light Yield (photons/keV) Measured at 662 keV, fwhm Energy Resolution (E%) Measured at 662 keV, Decay Time Constant (τ_{dec} (ns)), Peak Emission Wavelength (λ_{em} (nm)), Mass Density (g/cm^3), $\rho Z_{eff}^{3.5}$ Calculated Based on Tabulated Compound Composition and Mass Density, Pulse Duration Calculated Assuming a SiPM Recharge Time Constant of 7 ns (t_{FWHM} (ns)), and Pulse Quality Calculated Based on Tabulated Values of the Light Yield and Pulse Duration (PQ (photons/keV/ns)$^{1/2}$) of Plastic Scintillators

Compound	Light yield (Ph/keV)	E% @662 keV	τ_{dec} (ns)	λ_{em} (nm)	Density (g/cm^3)	$\rho Z_{eff}^{3.5}$ (10^6)	t_{fwhm} (ns)	PQ (Ph/keV/ns)$^{1/2}$	ref
Anthracene	20	n.r.	31	460	1.25	-[b]	39.7	0.712	329,330
Stilbene	16	n.r.	6	390	0.97	-[b]	15.9	1.005	329,331
p-Terphenyl	19	n.r.	7.2[a]	410	1.24	-[b]	17.4	1.057	329,332
Polyvinylcarbazole:Bi	12	9%	15	420	n.r.	-[b]	25.6	0.684	333
BC-400	13	n.r.	2.4	423	1.02	-[b]	10.5	1.113	334
BC-408	13	n.r.	2.1	425	1.02	-[b]	10.0	1.143	335
BC-412	12	n.r.	3.3	434	1.02	-[b]	12.0	1.000	336
BC-428	7.2	n.r.	12.5	480	1.02	-[b]	23.2	0.558	337
BC-430	9	n.r.	16.8	580	1.02	-[b]	27.3	0.574	338
BC-452	10	n.r.	2.1	424	1.05	-[b]	10.0	1.003	339
EJ-200	10	n.r.	2.1	425	1.02	-[b]	10.0	1.003	340
EJ-240	6.3	n.r.	285	430	1.02	-[b]	227	0.166	341
EJ-260	9.2	n.r.	9.2	490	1.02	-[b]	19.7	0.684	342
EJ-256	6.8	n.r.	2.1	425	1.08	-[b]	10.0	0.827	343

[a]Decay consists of multiple components; the tabulated value was calculated using eq 16. The amplitudes and decay times of the different components can be found in Table S6. [b]Effective atomic number could not be calculated due to lack of information on composition.

validated model of van der Sar et al. to simulate detector output pulses.[22−25]

Figure 5a shows the calculated variation of the pulse quality along the quenching curve. The pulse duration plotted on the *X*-axis is normalized by dividing it by the recharge time of the SiPM. A selection of simulated detector output pulses is shown in Figure 5b. The data points in 5a and the simulated pulses in Figure 5b can be grouped into three different regimes, based on the recharge and decay time. In regime (1), $\tau_{dec} \gg \tau_{rech}$. Quenching of the decay time in this regime results in a decrease of the pulse duration with almost no change of the pulse amplitude and therefore the pulse quality. In regime (2), $\tau_{dec} \approx$

https://doi.org/10.1021/acs.chemmater.4c03437
Chem. Mater. 2025, 37, 1716−1740

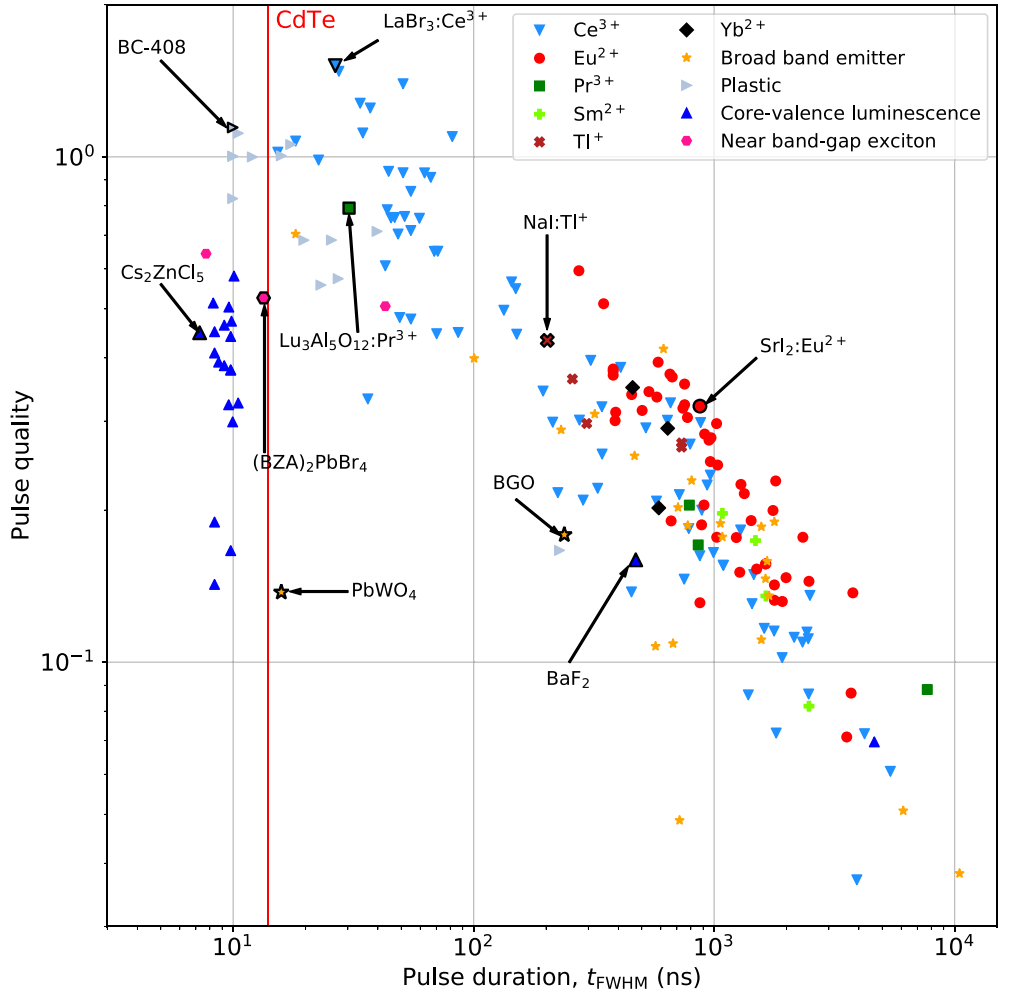

Figure 3. Plot of the pulse duration (t_{fwhm}) versus the pulse quality for Ce^{3+}-, Pr^{3+}-, Eu^{2+}-, Yb^{2+}-, Sm^{2+} codoped, and Tl^{+}-doped scintillators, intrinsic scintillators showing core−valence luminescence, broad-band emission, near band gap exciton emission, and plastic scintillators. The values of t_{fwhm} are calculated assuming a SiPM recharge time of 7 ns.

τ_{rech}. Quenching of the decay time in this regime results in a decrease of the pulse duration together with a moderate decrease in the amplitude of the simulated pulses and, therefore, the pulse quality. In regime (3), $\tau_{dec} \ll \tau_{rech}$. Quenching the decay time in this regime results in almost no decrease of the pulse duration but leads to a significant decrease of the pulse amplitude and, therefore, the pulse quality. In Figure 5a, this can be observed by the curve reaching a vertical asymptote along which only the pulse quality decreases. This behavior can also be observed in the simulated detector output pulses in Figure 5b. Ideally, a scintillator should thus be quenched from the first to the second regime, since further quenching of the decay time to the third regime will mostly result in a decrease of the total pulse intensity with almost no improvement of the pulse duration.

The single-barrier Arrhenius equation, assumed above, shows that there are two options to quench a scintillator, either by increasing the temperature (T) or by decreasing the energy barrier (ΔE). Given the requirement of room temperature operation, the only viable option is to decrease the energy barrier, i.e., decreasing the quenching temperature T_{50}, which represents the temperature at which the quenching curve reaches 50% of its maximum intensity.

The energy barrier, or T_{50}, can be changed via material engineering; this can also be referred to as T_{50}-engineering. An example of this can be found in the family of Ce^{3+}-doped garnets. Depending on the cation composition, thermal quenching can either take place through thermal ionization to the conduction band or interconfigurational crossover from the 5d excited state to the 4f ground state.[156,157] The activation energy of both processes strongly depends on composition and T_{50} values can be gradually tuned down from approximately 650 K in $Y_3Al_5O_{12}:Ce^{3+}$ to well below room temperature in $Y_3Ga_5O_{12}:Ce^{3+}$.[158] By replacing Al^{3+} with Ga^{3+}, the room temperature decay time could be shortened from approximately 80 to 18.6 ns.[159]

This is only one example of a system for which the quenching temperature can be engineered. As shown in Figure 3, there are a number of Ce^{3+}-doped materials with pulse durations approaching that of CdTe that could be improved and tailored via this approach. This can, however, also be used for intrinsic broad-band emitting scintillators. One of the main question of T_{50}-engineering is how the nonproportionality of the scintillator will be influenced. In principle, changes in composition should lead to minimal changes of the nonproportionality, but this needs to be confirmed experimentally.

VI.B. Co-doping. A more commonly used strategy to engineer or fine-tune the properties of a scintillator is to add additional dopants, also referred to as codoping.[160,161] Even

https://doi.org/10.1021/acs.chemmater.4c03437
Chem. Mater. 2025, 37, 1716−1740

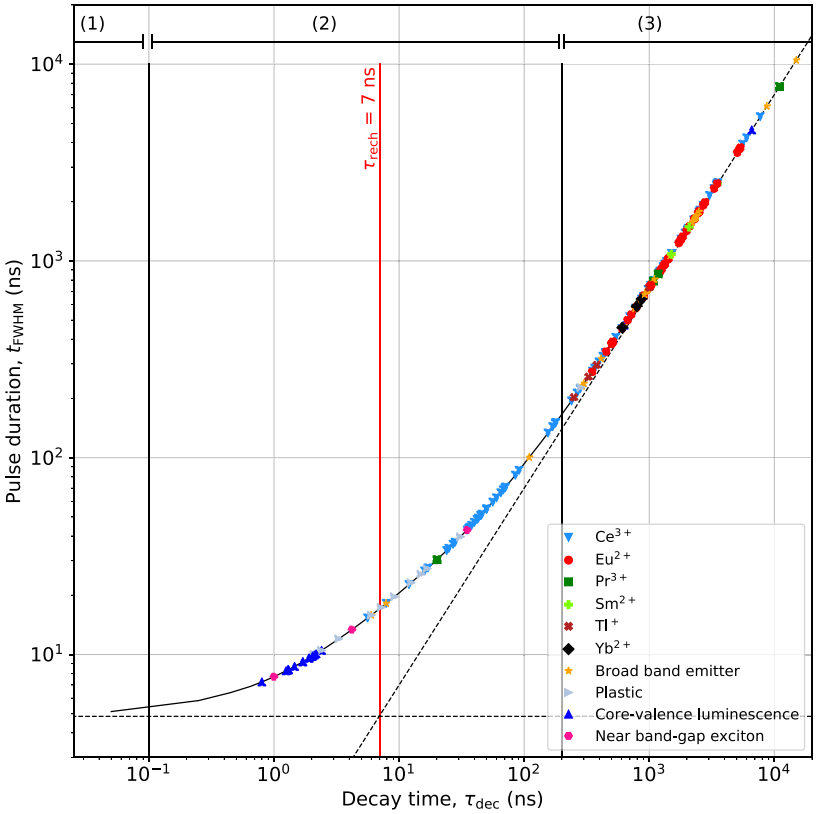

Figure 4. Scintillation decay time (τ_{dec}) versus calculated pulse duration (t_{fwhm}) for Ce^{3+}-, Pr^{3+}-, Eu^{2+}-, Yb^{2+}-, Sm^{2+} codoped, and Tl^{+}-doped scintillators, intrinsic scintillators showing core−valence luminescence, broad-band emission, near band gap exciton emission, and plastic scintillators. The red vertical line indicates the recharge time of the SiPM. The numbers (1), (2), and (3) indicate the regimes where $t_{fwhm}(\tau_{rech})$, $t_{fwhm}(\tau_{rech},\tau_{dec})$, and $t_{fwhm}(\tau_{dec})$. The two black vertical lines deliniate the different regimes.

high-quality scintillation crystals contain several different types of lattice defects, i.e., point defects, interstitials, dislocations, etc. The formation of such defects cannot completely be suppressed by optimizing the synthesis procedure. However, the influence of these defects can be mitigated via the addition of a specific codopant. This approach has for example been used to improve the nonproportionality of $LaBr_3:Ce^{3+}$ via codoping with Sr^{2+},[26,49,162] or $SrI_2:Eu^{2+}$ and $KCaI_3:Eu^{2+}$ by codoping with Zr^{4+}.[163,164] Co-doping can also be used to reduce afterglow, for example in $Gd_2O_2S:Pr^{3+}$[165] and $CsI:Tl^{+}$.[166−171] Other interesting examples are the improvement of the temporal response of the lutetium- and yttrium-based orthosilicates ($(Lu,Y)_2SiO_5:Ce^{3+}$) codoped with Ca^{2+}[51,172−174] and the garnets ($(Gd,Lu,Y)_3(Al,Ga)_5O_{12}:Ce^{3+}$) codoped with Mg^{2+}.[175−179]

It should be noted that the influence of a codopant is very hard to predict and that codopants can have multiple effects at the same time. A good example of this is $LaBr_3:Ce^{3+},Sr^{2+}$. On the one hand, codoping with Sr^{2+} improves the light yield and nonproportionality. On the other hand, it introduces multiple slower decay components, which is detrimental for application in an indirect PCD. The codoping approach thus requires a careful evaluation of the effects on all material properties.

VI.C. Dielectric Engineering. The hybrid organic−inorganic perovskites and perovskite-related compounds are an emerging group of intrinsic scintillators. These compounds can be engineered in many different ways, for example by doping the inorganic layer or by using a mix of organic molecules.[180−189] Another approach to engineer these materials is by changing the dielectric constant of the organic layer. This approach has been explored by Xia et al., who replaced phenethylammonium (PEA) on the A site of PEA_2PbBr_4 with benzimidazole (BM).[125] This approach is referred to as dielectric engineering.[125,126] The dielectric constant of BM is smaller than that of PEA; this enhances the exciton confinement by increasing the exciton binding energy and decreasing the exciton lifetime. Xia et al. report a scintillation decay time of 3.22 ns for $PEA(_2PbBr_4$, which decreases to 0.97 ns for BM_2PbBr_4. It should be noted that both of these compounds are still near-bandgap excitonic emitters, which means that self-absorption would still pose a challenge. Nonetheless, this approach may be very interesting for future developments in this class of hybrid organic−inorganic materials.

VII. CONCLUSIONS

The suitability of different types of scintillators for application in indirect PCDs has been assessed using three figures of merit: pulse intensity, pulse duration, and pulse quality. Based on these figures of merit, which are based on emissive properties, it is concluded that Ce^{3+}- or Pr^{3+}-doped materials form interesting classes of scintillators. Other groups that look promising are near band gap exciton emitters, plastics, and core−valence emitters. The application of these materials, however, is hampered by secondary problems or challenges, e.g., the match between the emission wavelength and PDE of the SiPM, presence of slow decay components, density, or nonproportionality. Examples are given of how scintillators can be engineered to optimize their emissive characteristics for use in indirect PCDs. If T50 engineering is used, the decay time of the scintillator should be quenched to values approximately similar to the recharge

https://doi.org/10.1021/acs.chemmater.4c03437
Chem. Mater. 2025, 37, 1716−1740

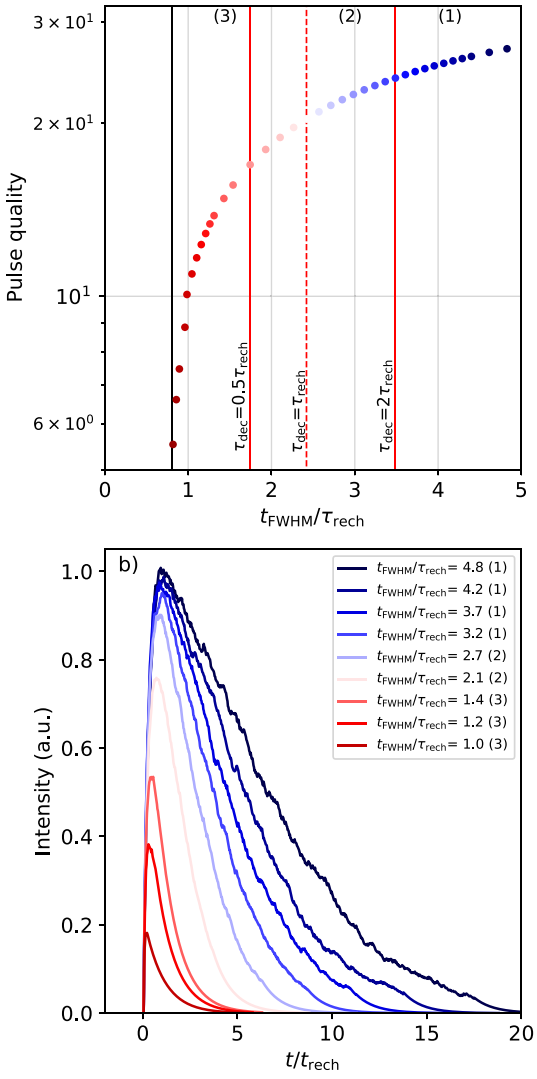

Figure 5. (a) t_{fwhm}/τ_{rech} versus the pulse quality, determined from simulated pulses, for different points along the quenching curve of a scintillator. (b) Selection of the simulated detector output pulses along the curve shown in (a). The numbers (1), (2), and (3) indicate the regimes in which $\tau_{dec} \gg \tau_{rech}$, $\tau_{dec} \approx \tau_{rech}$, and $\tau_{dec} \ll \tau_{rech}$, respectively.

time of the SiPM. Further quenching will lead to a decrease in the pulse intensity without any gain in pulse duration. This illustrates how choosing and/or engineering a suitable material for an indirect PCD depends on not only the material properties; the properties of the SiPM are just as important.

■ ASSOCIATED CONTENT

Supporting Information

The Supporting Information is available free of charge at https://pubs.acs.org/doi/10.1021/acs.chemmater.4c03437.

Decay times and amplitudes of scintillators for which an average decay time is tabulated (PDF)

■ AUTHOR INFORMATION

Corresponding Authors

J. Jasper van Blaaderen − *Delft University of Technology, Faculty of Applied Sciences, Department of Radiation Science and Technology, 2629 JB Delft, The Netherlands;* orcid.org/0000-0003-1460-8319; Email: j.j.vanblaaderen@tudelft.nl

Dennis R. Schaart − *Delft University of Technology, Faculty of Applied Sciences, Department of Radiation Science and Technology, 2629 JB Delft, The Netherlands; Holland Proton Therapy Center, 2629 JH Delft, The Netherlands;* Email: d.r.schaart@tudelft.nl

Authors

Casper van Aarle − *Delft University of Technology, Faculty of Applied Sciences, Department of Radiation Science and Technology, 2629 JB Delft, The Netherlands*

David Leibold − *Delft University of Technology, Faculty of Applied Sciences, Department of Radiation Science and Technology, 2629 JB Delft, The Netherlands*

Pieter Dorenbos − *Delft University of Technology, Faculty of Applied Sciences, Department of Radiation Science and Technology, 2629 JB Delft, The Netherlands*

Complete contact information is available at: https://pubs.acs.org/10.1021/acs.chemmater.4c03437

Notes

The authors declare no competing financial interest.

Biographies

J. Jasper van Blaaderen obtained his PhD in the department of Radiation Science & Technology at the Delft University of Technology. His research focuses on the development and exploration of small bandgap halide scintillators and the application of scintillator materials in scintillator-SiPM based indirect photon-counting X-ray detectors.

Casper van Aarle obtained his PhD in the department of Radiation Science & Technology at the Delft University of Technology. His research focused on the development of near-infrared emitting scintillator materials for gamma-ray spectroscopy.

David Leibold is a PhD student in the department of Radiation Science & Technology at the Delft University of Technology. His research focuses on the optimization of multienergy cone-beam CT for proton therapy.

Pieter Dorenbos is a full professor in luminescence materials research in the department of Radiation Science & Technology at the Delft University of Technology. He has a lifelong career in the development of new scintillation materials and fundamental studies of scintillation and luminescence mechanisms. Among other inventions, the widely applied $LaBr_3:Ce^{3+}$ scintillator was discovered in projects under his guidance. He also authored many papers on lanthanide level location in the bandgap of compounds.

Dennis R. Schaart heads the section Medical Physics & Technology at the department of Radiation Science & Technology at the Delft University of Technology. His research focuses on novel radiation detection technologies for medical imaging, image-guided interventions, and (proton) radiotherapy.

■ ACKNOWLEDGMENTS

The author acknowledge financial supports from the Dutch Research Council (TTW/OTP grant no. 18040), Varian, a Siemens Healthineers company (grant no. 2018016), and the European union (Horizon Europe grant no. 101112053) .

■ REFERENCES

(1) Flohr, T.; Petersilka, M.; Henning, A.; Ulzheimer, S.; Ferda, J.; Schmidt, B. Photon-counting CT review, Physica Medica. *Physica Medica* **2020**, *79*, 126−136.

(2) Roy, U. N.; Camarda, G. S.; Cui, Y.; Gul, R.; Hossain, A.; Yang, G.; Zazvorka, J.; Dedic, V.; Franc, J.; James, R. B. Role of selenium addition to CdZnTe matrix for room-temperature radiation detector applications. *Sci. Rep.* **2019**, *9*, 1620.
(3) Persson, M.; Bujila, R.; Nowik, P.; Andersson, H.; Kull, L.; Andersson, J.; Bornefalk, H.; Danielsson, M. Upper limits of photon fluence rate on CT detectors: Case study on a commercial scanner. *Medical Physics* **2016**, *43*, 4398−4411.
(4) Danielsson, M.; Persson, M.; Sjölin, M. M. sjolin, Photon-counting X-ray detectors for CT. *Phys. Med. Biol.* **2021**, *66*, No. 03TR01.
(5) Taguchi, K.; Iwanczyk, J. S. Vision 20/20: Single photon counting X-ray detectors in medical imaging. *Medical Physics* **2013**, *40*, 10.
(6) Willemink, M. J.; Persson, M.; Pourmorteza, A.; Pelc, N. J.; Fleischmann, D. Photon-counting CT: Technical principles and clinical prospects. *Radiology* **2018**, *289*, 293.
(7) Leng, S.; Bruesewitz, M.; Tao, S.; Rajendran, K.; Halaweish, A. F.; Campeau, N. G.; Fletcher, J. G.; McCollough, C. H. Photon-counting detector CT: system design and clinical applications of an emerging technology. *Radiographics* **2019**, *39*, 729.
(8) Hsieh, S. S.; Leng, S.; Rajendran, K.; Tao, S.; McCollough, C. H. Photon counting CT: Clinical Applications and Future Developments. *IEEE Transactions on Radiation and Plasma Medical Science* **2021**, *5*, 441.
(9) Kappler, S., Henning, A., Kreisler, B., Schoeck, F., Stierstorfer, K., Flohr, T. Photon counting CT at elevated X-ray tube currents: contrast stability, image noise and multi-energy performance. *Proceedings Volume 9033, Medical Imaging 2014: Physics of Medical Imaging*, 90331C, DOI: 10.1117/12.2043511.
(10) Steadman, R.; Herrmann, C.; Livne, A. ChromAIX2: A large area, high count-rate energy-resolving photon counting ASIC for a spectral CT prototype, Nuclear Instruments and Methods in Physics Research Section A: Accelerators, Spectrometers. *Detectors and Associated Equipment* **2017**, *862*, 18−24.
(11) Da Silva, J.; Gronberg, F.; Cederstrom, B.; Persson, M.; Sjolin, M.; Alagic, Z.; Bujila, R.; Danielsson, M. Resolution characterization of a silicon-based, photon-counting computed tomography prototype capable of patient scanning. *Journal of Medical Imaging* **2019**, *6*, 043502.
(12) Esquivel, A.; Ferrero, A.; Mileto, A.; Baffour, F.; Horst, K.; Rajiah, P. S.; Inoue, A.; Leng, S.; McCollough, C.; Fletcher, J. G. Photon-Counting detector CT: Key points radiologists should know. *Korean Journal of Radiology* **2022**, *23*, 854−865.
(13) Steadman, R.; Herrmann, C.; Mulhens, A.; Maeding, D. G. ChromAIX: Fast photon-counting ASIC for spectral computed tomography, Nuclear Instruments and Methods in Physics Research Section A: Accelerators, Spectrometers. *Detectors and Associated Equipment* **2011**, *648*, s211−s215.
(14) Taguchi, K.; Schaart, D. R.; Goorden, M. C.; Hsieh, S. S. Imaging performance of a $LaBr_3$:Ce scintillation detector for photon counting X-ray computed tomography: simulation study. *International Journal of Medical Physics Research and Practice* **2025**, *52*, 158.
(15) Persson, M.; Huber, B.; Karlsson, S.; Liu, X.; Chen, H.; Xu, C.; Yveborg, M.; Bornefalk, H.; Danielsson, M. Energy-resolved CT imaging with a photon-counting silicon-strip detecto. *Phys. Med. Biol.* **2014**, *59*, 6709.
(16) van Eijk, C. W. E. Inorganic Scintillators in Medical Imaging. *Phys. Med. Biol.* **2002**, *47*, R85.
(17) van Eijk, C. W. E. Inorganic Scintillators in medical imaging detectors. *Nuclear Instruments and Methods in physics Research Section A: Accelerators, Spectrometers, Detectors, and Associated Equipment* **2003**, *509*, 17.
(18) Lu, L.; Sun, M.; Lu, Q.; Wu, T.; Huang, B. High energy S-ray radiation sensitive scintillating materials for medical imaging, cancer diagnosis and terapy. *Nano energy* **2021**, *79*, No. 105437.
(19) Lecoq, P. Development of new scintillators for medical applications, Nucelar Instruments and Methods in Physics Research Section A: Accelerators, Spectrometers. *Detectors and Associated Equipment* **2016**, *809*, 130−139.
(20) Ronda, C.; Wieczorek, H.; Khanin, V.; Rodnyi, P. Review - Scintillators for medical imaing: a tutorial overview. *ECS Journal of Solid State Science and Technology* **2016**, *5*, R3121.
(21) van Loef, E. V.; Shah, K. S. Advances in scintillators for medical imaging applications. *Proceedings Volume 9214, Medical Applications of Radiation DetectorsIV* **2014**, 92140A.
(22) van der Sar, S. J. *Exploring X-ray photon-counting scintillation detectors with silicon photomultiplier readout for medical imaging*, ISBN: 978-94-6384-485-7, DOI: 10.4233/uuid:370aa87c-3055-4b2d-9e9e-ca74f2fab2e4.
(23) van der Sar, S. J.; Brunner, S. E.; Schaart, D. R. silicon photomultiplier-based scintillation detectors for photon-counting CT: A feasibility study. *Medical Physics* **2021**, *48*, 6324−6338.
(24) van der Sar, S. J.; Leibold, D.; Brunner, S. E.; Schaart, D. R. LaBr3:Ce and silicon photomultipliers: towards optimal scintillating photon-counting detector. *Proceedings Volume 12304, 7th International conference on Image Formation in X-ray Computed Tomography* **2022**, No. 12304A.
(25) van der Sar, S. J.; Brunner, S.; Schaart, D. X-ray photon-counting using silicon photomultiplier-based scintillation detectors at high X-ray tube currents. *Proceedings Volume 12031, Medical Imaging 2022: Physics of Medical Imaging*; 2022, 1203101;
(26) Alekhin, M. S.; Biner, D. A.; Kramer, K. W.; Dorenbos, P. Improvement of $LaBr_3$: 5% Ce scintillation properties by Li^+, Na^+, Mg^{2+}, Ca^{2+}, Sr^{2+}, and Ba^{2+} co-doping. *J. Appl. Phys.* **2013**, *113*, No. 224904.
(27) Arimoto, M.; Morita, H.; Fujieda, K.; Maruhashi, T.; Kataoka, J.; Nitta, H.; Ikeda, H. Development of LSI for a new kind of photon-counting computed tomography using multipixel photon counters. *Nuclear Instruments and methods in Physics Research Section A: Accelerators, Spectrometers, Detectors, and Associated Equipment* **2018**, *912*, 186.
(28) Kiji, H.; Maruhashi, T.; Toyoda, T.; Kataoka, J.; Arimoto, M.; Sato, D.; Yoshiura, K.; Kobayashi, S.; Kawashima, H.; Terazawa, S.; Shiota, S.; Ikeda, H. 64-Channel photon-counting computed tomography using a new MPPC-CT system. *Nuclear Instruments and methods in Physics Research Section A: Accelerators, Spectrometers, Detectors, and Associated Equipment* **2020**, *984*, 164610.
(29) Maruhashi, T.; Morita, H.; Arimoto, M.; Kataoka, J.; Fujieda, K.; Nitta, H.; Ikeda, H.; Kiji, H. Evaluation of a novel photon-counting CT system using a 16-channel MPPC array for multicolor 3-D imaging. *Nuclear Instruments and methods in Physics Research Section A: Accelerators, Spectrometers, Detectors, and Associated Equipment* **2019**, *936*, 5.
(30) Sato, D.; Arimoto, M.; Ishiguro, A.; Lucyana, F.; Tomoda, T.; Okumura, K.; Kawashima, H.; Kobayashi, S.; Murakami, K.; Kataoka, J.; Sagisaka, M.; Terazawa, S.; Shiota, S. Multi-energy in-vivo imaging of multiple contrast agents in a mouse using MPPC-based photon-counting CT. *Nuclear Instruments and Methods in Physics Reserach Section A: Accelerators, Spectromoeters, Detectors and Associated Equipment Detectors and Associated Equipment* **2024**, *1064*, No. 169337.
(31) Shimazoe, K.; Kim, D.; Hamdan, M.; Kobayashi, Y.; Kamada, K.; Yoshino, M.; Shoji, Y.; Sakamoto, K.; Acerbi, F.; Gola, A. Scintillator-single-photon avalanche diode array-based energy resolving photon counting X-ray detector. *communications engineering* **2024**, *3*, 167.
(32) van Dam, H. T.; Seifert, S.; Vinke, R.; Dendooven, P.; Lohner, H.; Beekman, F. J.; Schaart, D. R. A comprehensive model of the response of silicon photomultipliers. *IEEE Trans. Nucl. Sci.* **2010**, *57*, 2254.
(33) Dorenbos, P. The quest for high resolution y-ray scintillators. *Optical Materials: X* **2019**, *1*, No. 100021.
(34) Dorenbos, P. Fundamental limitations in the performance of Ce^{3+}-, Pr^{3+}-, and Eu^{2+}- activated scintillators. *IEEE Trans. Nucl. Sci.* **2010**, *57*, 1162.
(35) Dorenbos, P.; de Haas, J. T. M.; van Eijk, C. W. E. Non-proportionality in the scintillation response and the energy resolution obtainable with scintillation crystals. *IEEE Trans. Nucl. Sci.* **1995**, *42*, 2190.
(36) Moszynski, M. Inorganic scintillation detectors in y-ray spectrometry. *Nuclear Instruments and Methods in Physics Research*

Section A: Accelerators, Spectrometers, Detectors, and Associated Equipment, **2003**, *505*, 101−110.
(37) Rodnyi, P. A.; Dorenbos, P.; van Eijk, C. W. E. Energy loss in inorganic scintillators. *Physica Status solidi b* **1995**, *187*, 15.
(38) khodyuk, I. V.; Rodnyi, P. A.; Dorenbos, P. Nonproportional scintillation response of NaI:Tl to low energy X-ray photons and electrons. *J. Appl. Phys.* **2010**, *107*, 11.
(39) Khodyuk, I. V.; Dorenbos, P. nonproportional response of $LaBr_3$:Ce and $LaCl_3$:Ce scintillators to synchrotron X-ray irradiation. *J. Phys.: Condens. Matter* **2010**, *22*, 485402.
(40) Khodyuk, I. V.; de Haas, J. T. M.; Dorenbos, P. Nonproportional response between 0.1−100 keV energy by means of highly monochromatic synchrotron X-rays. *IEEE Trans. Nucl. Sci.* **2010**, *57*, 1175.
(41) Moszynski, M. Energy resolution and non-proportionality of scintillation detectors - new observations. *Radiation measurements* **2010**, *45*, 372−376.
(42) Bizarri, G.; Cherepy, N. J.; Choong, W. S.; Hull, G.; Moses, W. W.; Payne, S. A.; Singh, J.; Valentine, J. D.; Vasilev, A. N.; Williams, R. T. Progress in studying scintillator proportionality: Phenomenlogical model. *IEEE Trans. Nucl. Sci.* **2009**, *56*, 2313.
(43) Grim, J. Q.; Ucer, K. B.; Burger, A.; Bhattacharya, P.; Tupitsyn, E.; Rowe, E.; Buliga, V. M.; Trefilova, L.; Gektin, A.; Bizarri, G. A.; Moses, W. W.; Williams, R. T. Nonlinear quenching of densely excited states in wide-gap solids. *Physcial Review B* **2013**, *87*, No. 125117.
(44) Williams, R. T.; Grim, J. Q.; Li, Q.; Ucer, K. B.; Moses, W. W. Excitation density, diffusion-drift, and proportionality in scintillators. *Physica Status Solidi b* **2011**, *248*, 426.
(45) Lu, X.; Gridin, S.; Williams, R. T.; Mayhugh, M. R.; Gektin, A.; Syntfeld-Kazuch, A.; Swiderski, L.; Moszynski, M. Energy-dependent scintillation pulse shape and proportionality of decay components for CsI:Tl: modeling with transport and rate equations. *Physical Review Applied* **2017**, *7*, No. 014007.
(46) Magdowski, M.; Vick, R. Estimation of the mathematical parameters of double-exponential pulses using the nelder-mead algorithm. *IEEE Transactions on Electromagnetic Compatibility* **2010**, *52*, 1060.
(47) Camp, M.; garbe, H. Parameter estimation of double exponential pulses (EMP, UWB) with least squares and nelder mead algoritm. *IEEE Transactions on Electromagnetic Compatibillity* **2004**, *46*, 675.
(48) Bos, A. J. J.; Draaisma, F. S.; Okx, W. J. C. Hoofdstuk 3: Wisselwerking can straling met materie. *Inleiding tot de Stralingshygiene, Sdu Uitgevers*; 2007, 64, ISBN: 978-90-12-11-905-4
(49) Alekhin, M. S.; de Haas, J. T. M.; Khodyuk, I. V.; Kramer, K. W.; Menge, P. R.; Ouspenski, V.; Dorenbos, P. Improvement of y-ray energy resolution of $LaBr_3$:Ce^{3+} scintillation detectors by Sr^{2+} and Ca^{2+} co-doping. *Appl. Phys. Lett.* **2013**, *102*, No. 161915.
(50) Melcher, C. L.; Schweitzer, J. S. Cerium-doped lutetium oxyorthosilicate: a fast, efficient new scintillator. *IEEE Trans. Nucl. Sci.* **1992**, *39*, 502.
(51) Spurrier, M. A.; Szupryczynski, P.; Yang, K.; Carey, A. A.; Melcher, C. L. Effects of Ca^{2+} co-doping on the scintillation properties of LSO:Ce. *IEEE Trans. Nucl. Sci.* **2008**, *55*, 1178.
(52) de Haas, J. T. M.; Dorenbos, P. Advances in Yield calibration of scintillators. *IEEE Trans. Nucl. Sci.* **2008**, *55*, 1086.
(53) Pepin, C. M.; Berard, P.; Perrot, A.-L.; Pepin, C.; Houde, D.; Lecomte, R.; Melcher, C. L.; Dautet, H. Properties of LYSO and recent LSO scintillators for phoswich PET detectors. *IEEE Trans. Nucl. Sci.* **2004**, *51*, 789.
(54) Data Sheet Luxium Solutions LYSO, Obtained February 2024, https://luxiumsolutions.com/radiation-detection-scintillators/crystal-scintillators/lysoscintillation-crystals.
(55) Schaart, D. R. Physics and technology of time-of-flight PET detectors. *Phys. Med. Biol.* **2021**, *66*, No. 09TR01.
(56) Smith, M. B.; Achtzehn, T.; Andrews, H. R.; Clifford, E. T. H.; Forget, P.; Glodo, J.; Hawrami, R.; Ing, H.; O'Dougherty, P.; Shah, K. S.; Shirwadkar, U.; Soundara-Pandian, L.; Tower, J. Fast neutron measurements using Cs_2LiYCl_6 (CLYC) scintillator. *Nuclear Instruments and Methods in Physics Research Section A: Accelerators, Spectrometers, Detectors and Associated Equipment* **2015**, *784*, 162−167.
(57) D'Olympia, N.; Chowdhury, P.; Lister, C. J.; Glodo, J.; Hawrami, R.; Shah, K.; Shirwadkar, U. Pulse-shape analysis of CLYC for thermal neutrons, fast neutrons, and gamma-rays. *Nuclear Instruments and Methods in Physics Research Section A: Accelerators, Spectrometers, Detectors and Associated Equipment* **2013**, *714*, 121−127.
(58) Bourne, M. M.; Mussi, C.; Miller, E. C.; Clarke, S. D.; Pozzi, S. A.; gueorguiev, A. Characterisation of the CLYC detector for neutron and photon detection. *Nuclear Instruments and Methods in Physics Research Section A: Accelerators, Spectrometers, Detectors and Associated Equipment* **2014**, *736*, 124−127.
(59) Cherepy, N. J.; Hull, G.; Drobshoff, A. D.; Payne, S. A.; van Loef, E.; Wilson, C. M.; Shah, K. S.; Roy, U. N.; Burger, A.; Boatner, L. A.; Choong, W.-S.; Moses, W. W. Strontium and barium iodide high light yield scintillators. *Appl. Phys. Lett.* **2008**, *92*, 8.
(60) Boatner, L. A.; Ramey, J. O.; kolopus, J. A.; Hawrami, R.; Higgins, W. M.; van Loef, E.; Glodo, J.; Shah, K. S.; Rowe, E.; Bhattacharya, P.; Tupitsyn, E.; Groza, M.; Burger, A.; Cherepy, N. J.; Payne, S. A. Bridgman growth of large SrI_2:Eu^{2+} single crystals: A high-performance scintillator for radiation detection applications. *J. Cryst. Growth* **2013**, *379*, 63−68.
(61) Wilson, C. M.; van Loef, E. V.; Glodo, J.; Cherepy, N.; Hull, G.; Payne, S.; Choong, W.-S.; Moses, W.; Shah, K. S. Strontium iodide scintillators for high energy resolution gamma ray spectroscopy. *Proceedings Volume 7079, Hard X-ray, Gamma-Ray and Neutron Detector Physics X* **2008**, No. 707917.
(62) Bourret-Courchesne, E. D.; Bizarri, G.; Borade, R.; Yan, Z.; Hanrahan, S. M.; Gundiah, G.; Chaudhry, A.; Canning, A.; Derenzo, S. E. Eu^{2-}-doped Ba_2CsI_5, a new high-performance scintillator. *Nuclear Instruments and Methods in Physics Research Section A: Accelerators, Spectrometers, Detectors and Associated Equipment* **2009**, *612*, 138.
(63) Alekhin, M. S.; Biner, D. A.; Kramer, K. W.; Dorenbos, P. Optical and scintillation properties of $CsBa_2I_5$:Eu^{2+}. *J. Lumin.* **2014**, *145*, 723−728.
(64) Wu, Y.; Zhuravleva, M.; Lindsey, A. C.; Koschan, M.; Melcher, C. L. Eu^{2+} concentration effects in $KCa_{0.8}Sr_{0.2}I_3$:Eu^{2+}: A novel high-performance scintillator. *Nuclear Instruments and Methods in Physics Research Section A: Accelerators, Spectrometers, Detectors and Associated Equipment* **2016**, *820*, 132−140.
(65) Glodo, J.; van Loef, E. V.; Cherepy, N. J.; Payne, S. A.; Shah, K. S. Concentration Effects in Eu Doped SrI_2. *IEEE Trans. Nucl. Sci.* **2010**, *57*, 1228.
(66) Yang, K.; Zhuravleva, M.; Melcher, C. L. Crystal growth and characterization of $CsSr_{1-x}Eu_xI_3$ high light yield scintillators. *Physica Status Solidi Rapid Research Letters* **2011**, *5*, 43.
(67) Gundiah, G.; Gascon, M.; Bizarri, G.; Derenzo, S. E.; Bourret-Courchesne, E. D. Structure and scintillation of Eu^{2+}-activated calcium bromide iodide. *J. Lumin.* **2015**, *159*, 274−279.
(68) Alekhin, M. S.; Kramer, K. W.; Dorenbos, P. Self-absorption in SrI_2: 2% Eu^{2+} between 78 and 600 K. *Nuclear Instruments and Methods in Physics Research Section A: Accelerators, Spectrometers, Detectors and Associated Equipment* **2013**, *714*, 13−16.
(69) Suta, M.; Wickleder, C. Synthesis, spectroscopic properties and applications of divalent lanthanides apart from Eu^{2+}. *J. Lumin.* **2019**, *210*, 210.
(70) van Aarle, C.; Kramer, K. W.; Dorenbos, P. Lengthening of the Sm^{2+} 4f55d ? 4f6 decay time through interplay with the 4f6[5D0] level and its analogy to Eu^{2+} and Pr^{3+}. *J. Lumin.* **2024**, *266*, No. 120329.
(71) Awater, R. H. P.; Alekhin, M. S.; Biner, D. A.; Kramer, K. W.; Dorenbos, P. Converting SrI_2:Eu^{2+} into a near infrared scintillator by Sm^{2+} co-doping. *J. Lumin.* **2019**, *212*, 1−4.
(72) Wolszczak, W.; Kramer, K. W.; Dorenbos, P. $CsBa_2I_5$:Eu^{2+},Sm^{2+}—The First High-Energy Resolution Black Scintillator for y-Ray Spectroscopy. *Physica Status Solidi Rapid Research Letters* **2019**, *13*, 9.
(73) van Aarle, C.; Kramer, K. W.; Dorenbos, P. Avoiding concentration quenching and self-absorption in Cs_4EuX_6 (X = Br, I) by Sm^{2+} doping. *Journal of Materials Chemistry C* **2023**, *11*, 2336−2344.

https://doi.org/10.1021/acs.chemmater.4c03437
Chem. Mater. 2025, 37, 1716−1740

(74) van Aarle, C.; Kramer, K. W.; Dorenbos, P. Characterisation of Sm^{2+}-doped $CsYbBr_3$, $CsYbI_3$ and $YbCl_2$ for near-infrared scintillator application. *J. Lumin.* **2022**, *251*, No. 119209.
(75) van Aarle, C.; Kramer, K. W.; Dorenbos, P. The role of Yb^{2+} as a scintillation sensitiser in the near-infrared scintillator $CsBa_2I_5:Sm^{2+}$. *J. Lumin.* **2021**, *238*, No. 118257.
(76) Drozdowski, W.; Lukasiewicz, T.; Wojtowicz, A. J.; Wisniewski, D.; Kisielewski, J. Thermoluminescence and scintillation of praseodymium-activated $Y_3Al_5O_{12}$ and $LuAlO_3$ crystals. *J. Cryst. Growth* **2005**, *275*, e709.
(77) Sreebunpeng, K.; Chewpraditkul, W.; Babin, V.; Nikl, M.; Nejezchleb, K. Scintillation response of $Y_3Al_5O_{12}:Pr^{3+}$ single crystal scintillators. *Radiation Measurmeents* **2013**, *56*, 94−7.
(78) Ogino, H.; Yoshikawa, A.; Nikl, M.; Kamada, K.; Fukuda, T. Scintillation characteristics of Pr-doped $Lu_3Al_5O_{12}$ single crystals. *J. Cryst. Growth* **2006**, *292*, 239.
(79) Sreebunpeng, K.; Chewpraditkul, W.; Nikl, M. Luminescence and scintillation properties of Advanced $Lu_3Al_5O_{12}:Pr^{3+}$. *Radiat. Meas.* **2014**, *60*, 42−45.
(80) Nikl, M.; Ogino, H.; Krasnikov, A.; Beitlerova, A.; Yoshikawa, A.; Fukuda, T. Photo- and radioluminescence of Pr-Doped $Lu_3Al_5O_{12}$ single crystal, Physica status solidi a. *Applications and material science* **2005**, *202*, R4.
(81) Pejchal, J.; Nikl, M.; Mihokova, A.; Mares, J. A.; Yoshikawa, A.; Ogino, H.; Schillemat, K. M.; Krasnikov, A.; Vedda, A.; Nejezchleb, K.; Múčka, V. Pr^{3+} -doped complex oxide single crystal scintillators. *J. Phys. D: Appl. Phys.* **2009**, *42*, 055117.
(82) Srivastava, A. M. Aspects of Pr^{3+} luminescence in solids. *J. Lumin.* **2016**, *169*, 445.
(83) Zych, A.; de Lange, M.; de Mello Donega, C.; Meijerink, A. Analysis of the radiative lifetime of Pr^{3+} d-f emission. *J. Appl. Phys.* **2012**, *112*, 1.
(84) Ogino, H.; Yoshikawa, A.; Nikl, M.; Krasnikov, A.; Kamada, K.; Fukuda, T. Growth and scintillation properties of Pr-doped $Lu_3Al_5O_{12}$ crystals. *J. Cryst. Growth* **2006**, *287*, 335.
(85) Drozdowski, W.; Dorenbos, P.; de Haas, J. T. M.; Drozdowska, R.; Owens, A.; Kamada, K.; Tsutsumi, K.; Usuki, Y.; Yanagida, T.; Yoshikawa, A. Scintillation Properties of Praseodymium Activated $Lu_3Al_5O_{12}$ Single Crystals. *IEEE Trans. Nucl. Sci.* **2008**, *55*, 2420.
(86) Hawrami, R.; Ariesanti, E.; Farsoni, A.; Szydel, D.; Sabet, H. Growth and Evaluation of Improved CsI:Tl and NaI:Tl Scintillators. *Crystals* **2022**, *12*, 1517.
(87) Aitken, D. W.; Beron, B. L.; Yenicay, G.; zulliger, H. R. The Fluorescent Response of NaI(Tl), CsI(Tl), CsI(Na) and CaF_2(Eu) to X-Rays and Low Energy Gamma Rays. *IEEE Trans. Nucl. Sci.* **1967**, *14*, 468.
(88) Swiderski, L.; Moszynski, M.; Syntfeld-Kazuch, A.; Szawlowski, M.; Szczesniak, T. Measuring the scintillation decay time for different energy depositions in NaI:Tl, LSO:Ce and $CeBr_3$ scintillators. *Nuclear Instruments and Methods in Physics Research Section A: Accelerators, Spectrometers, Detectors and Associated Equipment* **2014**, *749*, 68−73.
(89) Hofstadter, R. Alkali Halide Scintillation Counters. *Physical Review Journals Archive* **1948**, *74*, 100.
(90) Hofstadter, R. The Detection of Gamma-Rays with Thallium-Activated Sodium Iodide Crystals. *Physical Review Journals Archive* **1949**, *75*, 796.
(91) Hofstadter, R.; Mcintyre, J. A. Measurement of Gamma-Ray Energies with Single Crystals of NaI(Tl). *Physical Review Journals Archive* **1950**, *80*, 631.
(92) Weber, S.; Christ, D.; Kurzeja, M.; Engels, R.; Kemmerling, G.; Halling, H. Comparison of LuYAP, LSO, and BGO as scintillators for high resolution PET detectors. *IEEE Trans. Nucl. Sci.* **2003**, *50*, 1370.
(93) Moszynski, M.; Gresset, C.; Vacher, J.; Odru, R. Timing properties of BGO scintillator. *Nucl. Instrum. Methods Phys. Res.* **1981**, *188* (2), 403.
(94) Brunner, S. E.; Schaart, D. R. BGO as a hybrid scintillator/Cherenkov radiator for cost-effective time-of-flight PET. *Physics in Medicin and Biology* **2017**, *62*, 4421.
(95) Lecoq, P.; Dafinei, I.; Auffray, E.; Schneegans, M.; Korzhik, M. V.; Missevitch, O. V.; Pavlenko, V. B.; Fedorov, A. A.; Annenkov, A. N.; Kostylev, V. L.; Ligun, V. D. Lead tungstate ($PbWO_4$) scintillators for LHC EM calorimetry. *Nuclear Instruments and Methods in Physics Research Section A: Accelerators, Spectrometers, Detectors and Associated Equipment* **1995**, *365* (2−3), 291.
(96) Moses, W. W. Current trends in scintillator detectors and materials. *Nuclear Instruments and Methods in physics Research Section A: Accelerators, Spectrometers, Detectors and Associated Equipment* **2002**, *487* (1−2), 123.
(97) Saeki, K.; Fujimoto, Y.; Koshimizu, M.; Yanagida, T.; Asai, K. Comparative study of scintillation properties of Cs_2HfCl_6 and Cs_2ZrCl_6. *Applied Physics Express* **2016**, *9*, No. 042602.
(98) Saeki, K.; Fujimoto, Y.; Koshimizu, M.; Nakauchi, D.; Tanaka, H.; Yanagida, T.; Asai, K. Luminescence and scintillation properties of Cs_2HfBr_6 and Cs_2ZrBr_6 crystals. *Jpn. J. Appl. Phys.* **2018**, *57*, No. 030310.
(99) Kodama, S.; Kurosawa, S.; Ohno, M.; Yamaji, A.; Yoshino, M.; Pejchal, J.; Kral, R.; Ohashi, Y.; Kamada, K.; Yokota, Y.; Nikl, M.; Yoshikawa, A. Development of a novel red-emitting cesium hafnium iodide scintillator. *Radiat. Meas.* **2019**, *124*, 54−58.
(100) Kodama, S.; Kurosawa, S.; Yamaji, A.; Pejchal, J.; kral, R.; Ohashi, Y.; Kamada, K.; Yokota, Y.; Nikl, M.; Yoshikawa, A. Growth and luminescent properties of Ce and Eu doped Cesium Hafnium Iodide single crystalline scintillators. *J. Cryst. Growth* **2018**, *492*, 1−5.
(101) van Blaaderen, J. J.; van den Brekel, L. A.; Kramer, K. W.; Dorenbos, P. Scintillation and Optical Characterization of $CsCu_2I_3$ Single Crystals from 10 to 400 K. *Chem. Mater.* **2023**, *35*, 9623.
(102) Cheng, S.; Beitlerova, A.; Kucerkova, R.; Mihokova, E.; Nikl, M.; Zhou, Z.; Ren, G.; Wu, Y. Non-Hygroscopic, Self-Absorption Free, and Efficient 1D $CsCu_2I_3$ Perovskite Single Crystal for Radiation Detection. *ACS Appl. Mater. Interfaces* **2021**, *13*, 12198.
(103) Cheng, S.; Beitlerova, A.; Kucerkova, R.; nikl, M.; Ren, G.; Wu, Y. Zero-Dimensional $Cs_3Cu_2I_5$ Perovskite Single Crystal as Sensitive X-Ray and y-Ray Scintillator. *Physica Status Solidi Rapid Research Letters* **2020**, *14*, 11.
(104) Hawrami, R.; Ariesanti, E.; Wei, H.; Finkelstein, J.; Glodo, J.; Shah, K. S. Intrinsic scintillators: $TlMgCl_3$ and $TlCaI_3$. *J. Cryst. Growth* **2017**, *475*, 216−219.
(105) Khan, A.; Rooh, G.; Kim, H. J.; Park, H.; Kim, S. Intrinsically activated $TlCaCl_3$: A new halide scintillator for radiation detection. *Radiat. Meas.* **2017**, *107*, 115−118.
(106) Hawrami, R.; Ariesanti, E.; Buliga, V.; Burger, A.; Lam, S.; Motakef, S. Tl_2HfCl_6 and Tl_2ZrCl_6: Intrinsic Tl-, Hf-, and Zr-based scintillators. *J. Cryst. Growth* **2020**, *531*, No. 125316.
(107) Fujimoto, Y.; Saeki, K.; Nakauchi, D.; Yanagida, T.; Koshimizu, M.; Asai, K. New Intrinsic Scintillator with Large Effective Atomic Number: Tl_2HfCl_6 and Tl_2ZrCl_6 Crystals for X-ray and Gamma-ray Detections. *Sens. Mater.* **2018**, *30*, 1577.
(108) van Blaaderen, J. J.; Biner, D.; Kramer, K. W.; Dorenbos, P. The temperature dependent optical and scintillation characterisation of Bridgman grown $CsPbX_3$ (X = Br, Cl) single crystals Nuclear Insturments and Methods in Physics Research Section A: Accelerators, Spectrometers. *Detectors and Associated Equipment* **2024**, *1064*, No. 169322.
(109) van Blaaderen, J. J.; van Hattem, A.; Mulder, J. T.; Biner, D.; Kramer, K. W.; Dorenbos, P. Photoluminescence and Scintillation Mechanism of Cs_4PbBr_6. *J. Phys. Chem. C* **2024**, *128* (46), 19921−19932.
(110) Mykhaylyk, V. B.; Kraus, H.; Kapustianyk, V.; Kim, H. J.; Mercere, P.; Rudko, M.; Da Silva, P.; Antonyak, O.; Dendebera, M. Bright and fast scintillations of an inorganic halide perovskite $CsPbBr_3$ crystal at cryogenic temperatures. *Sci. Rep.* **2020**, *10*, 8601.
(111) Mykhaylyk, V. B.; Rudko, M.; Kraus, H.; Kapustianyk, V.; Kolomiets, V.; Vitoratou, N.; Chornodolskyy, Y.; Voloshinovskii, A. S.; Vasylechko, L. Ultra-fast low temperature scintillation and X-ray luminescence of $CsPbCl_3$ crystals. *Journal of Materials Chemistry C* **2023**, *11*, 656−665.

https://doi.org/10.1021/acs.chemmater.4c03437
Chem. Mater. 2025, 37, 1716−1740

(112) Fratelli, A., Zaffalon, M. L., Mazzola, E., Dirin, D., Cherniukh, I., Martinez, C. O., Salomoni, M., Carulli, F., Meinardi, F., Gironi, L., Manna, L., Kovalenko, M. V., Brovelli, S. Size-dependent multiexciton dynamics governs scintillation from perovskite quantum dots, *ArXiv*, DOI: 10.48550/arXiv.2409.16994.
(113) Li, Y.; Shao, W.; Ouyang, X.; Zhu, Z.; Zhang, H.; Ouyang, X.; Liu, B.; Xu, Q. Scintillation Properties of Perovskite Single Crystals. *J. Phys. Chem. C* **2019**, *123*, 17449.
(114) Tang, Y.; Pu, G.; Tang, Y.; Sun, T.; Wang, M.; Wang, J. Recent Advances in Fast-Decaying Metal Halide Perovskites Scintillators. *J. Phys. Chem. Lett.* **2024**, *15*, 7036.
(115) Manny, T. F.; Shonde, T. B.; Liu, H.; Islam, M. S.; Olasupo, O. J.; Viera, J.; Moslemi, S.; Khizr, M.; Chung, C.; Winfred, J. S. R. V.; Stand, L. M.; Hilinski, E. F.; Schlenoff, J.; Ma, B. Efficient X-Ray Scintillators Based on Facile Solution Processed 0D Organic Manganese Bromide Hybrid Films. *Adv. Funct. Mater.* **2025**, *35*, No. 2413755.
(116) Xu, L.-J.; Lin, X.; He, Q.; Worku, M.; Ma, B. Highly efficient eco-friendly X-ray scintillators based on an organic manganese halide. *Nat. Commun.* **2020**, *11*, 4329.
(117) He, Q.; Zhou, C.; Xu, L.; Lee, S.; Lin, X.; Neu, J.; Worku, M.; Chaaban, M.; Ma, B. Highly Stable Organic Antimony Halide Crystals for X-ray Scintillation. *ACS Materials Letters* **2020**, *2*, 633.
(118) Morad, V.; Shynkarenko, Y.; Yakunin, S.; Brumberg, A.; Schaller, R. D.; Kovalenko, M. V. Disphenoidal Zero-Dimensional Lead, Tin, and Germanium Halides: Highly Emissive Singlet and Triplet Self-Trapped Excitons and X-ray Scintillation. *J. Am. Chem. Soc.* **2019**, *141*, 9764.
(119) Xie, A.; Maddalena, F.; Witkowski, M. E.; Makowski, M.; Mahler, B.; Drozdowski, W.; Springham, S. V.; Coquet, P.; Dujardin, C.; Birowosuto, M. D.; Dang, C. Library of Two-Dimensional Hybrid Lead Halide Perovskite Scintillator Crystals. *Chem. Mater.* **2020**, *32*, 8530−8539.
(120) Xie, A.; Hettiarachchi, C.; Maddalena, F.; Witkowski, M. E.; Makowski, M.; Drozdowski, W.; Arramel, A.; Wee, A. T. S.; Springham, S. V.; Vuong, P. Q.; Kim, H. J.; Dujardin, C.; Coquet, P.; Birowosuto, M. D.; Dang, C. Lithium-doped two-dimensional perovskite scintillator for wide-range radiation detection. *Communications Materials* **2020**, 37.
(121) Birowosuto, M. D.; Cortecchia, D.; Drozdowski, W.; Brylew, K.; Lachmanski, W.; Bruno, A.; Soci, C. X-ray Scintillation in Lead Halide Perovskite Crystals. *Sci. Rep.* **2016**, *6*, No. 37254.
(122) Wolszczak, W. W., Carrroll, D. L., Williams, R. T. *Advanced X-ray Detector Technologies*, Chapter 1, 2022, DOI: 10.1007/978-3-030-64279-2_1.
(123) Williams, R. T.; Wolszczak, W. W.; Yan, X.; Carroll, D. L. Perovskite Quantum-Dot-in-Host for Detection of Ionizing Radiation. *ACS Nano* **2020**, *14*, 5161−5169.
(124) van Blaaderen, J. J.; van der Sar, S.; Onggo, D.; Sheikh, M. A. K.; Schaart, D. R.; Birowosuto, M. D.; Dorenbos, P. $BZA)_2PbBr_4$: A potential scintillator for photon-counting computed tomography detectors. *J. Lumin.* **2023**, *263*, No. 120012.
(125) Xia, M.; Xie, Z.; Wang, H.; Jin, T.; Liu, L.; Kang, J.; Sang, Z.; Yan, X.; Wu, B.; Hu, H.; Tang, J.; Niu, G. Sub-Nanosecond 2D Perovskite Scintillators by Dielectric Engineering. *Adv. Mater.* **2023**, *35*, 2211769.
(126) Chen, B.; Yu, R.; Xing, G.; Wang, Y.; Wang, W.; Chen, Y.; Xu, X.; Zhao, Q. Dielectric Engineering of 2D Organic-Inorganic Hybrid Perovskites. *ACS Energy Letters* **2024**, *9*, 226.
(127) Khanin, V.; Venevtsev, I.; Rodnyi, P. Recent advances in the study of core-valence luminescence (cross luminescence). *Review, Optical Materials* **2023**, *136*, No. 113399.
(128) Rodnyi, P. A.; Anderson, J. R. X. Core-valance band transitions in wide-gap ionic crystals. *Soviet Physics Solid State* **1992**, *34*, 7.
(129) Rodnyi, P. A. Choice of Compounds with Fast Core-Valence Transitions. *MRS Online Proceedings Library* **1994**, *348*, 77−88.
(130) Laval, M.; Moszynski, M.; Allemand, R.; Cormoreche, E.; Guinet, P.; Odru, R.; Vacher, J. Barium fluoride—Inorganic scintillator for subnanosecond timing, Nuclear Instruments and Methods in Physics Research. *Nucl. Instrum. Methods Phys. Res.* **1983**, *206* (1−2), 169.
(131) Rodnyi, P. A. Core−valence luminescence in scintillators. *Radiation measurments* **2004**, *38*, 343.
(132) Radzhabov, E.; Istomin, A.; Nepomnyashikh, A.; Egranov, A.; Ivashechkin, V. Exciton interaction with impurity in barium fluoride crystals. *Nuclear Instruments and Methods in physics Research Section A: Accelerators, Spectrometers, Detectors and Associated Equipment* **2005**, *537*, 71.
(133) Gundacker, S.; Pots, R. H.; Nepomnyashchikh, A.; Radzhabov, E.; Shendrik, R.; Omelkov, S.; Kirm, M.; Acerbi, F.; Capasso, M.; Paternoster, G.; Mazzi, A.; Gola, A.; Chen, J.; Auffray, E. Vacuum ultraviolet silicon photomultipliers applied to BaF_2 cross-luminescence detection for high-rate ultrafast timing applications. *Phys. Med. Biol.* **2021**, *66*, No. 114002.
(134) Hu, C.; Xu, C.; Zhang, L.; Zhang, Q.; Zhu, R.-Y. Development of Yttrium-Doped BaF_2 Crystals for Future HEP Experiments. *IEEE Trans. Nucl. Sci.* **2019**, *66*, 1854.
(135) Chen, J.; Yang, F.; Zhang, L.; Zhu, R.-Y.; Du, Y.; Wang, S.; Sun, S.; Li, X. Slow Scintillation Suppression in Yttrium Doped BaF_2 Crystals. *IEEE Trans. Nucl. Sci.* **2018**, *65*, 2147.
(136) Seliverstov, D. M.; Demidenko, A. A.; Garibin, E. A.; Gain, S. D.; Gusev, Y. I.; Fedorov, P. P.; Kosyanenko, S. V.; Mironov, I. A.; Osiko, V. V.; Rodnyi, P. A.; Smirnov, A. N.; Suvorov, V. M. New fast scintillators on the base of BaF_2 crystals with increased light yield of 0.9 ns luminescence for TOF PETt. *Nuclear Instruments and Methods in physics Research Section A: Accelerators, Spectrometers, Detectors and Associated Equipment* **2012**, *695*, 369−372.
(137) Rutstrom, D.; Stand, L.; Delzer, C.; Kapusta, M.; Glodo, J.; van Loef, E.; Shah, K.; Koschan, M.; Melcher, C. L.; Zhuravleva, M. Improved light yield and growth of large-volume ultrafast single crystal scintillators Cs_2ZnCl_4 and Cs_3ZnCl_5. *Opt. Mater.* **2022**, *133*, No. 112912.
(138) Rutstrom, D.; Stand, L.; Windsor, D.; Xu, H.; Kapusta, M.; Melcher, C. L.; Zhuravleva, M. New ultrafast scintillators with core valence luminescence: Cs_2MgCl_4 and Cs_3MgCl_5. *Journal of Materials Chemistry C* **2024**, *12*, 6920−6931.
(139) Rutstrom, D.; Stand, L.; Kapusta, M.; Windsor, D.; Xu, H.; Melcher, C. L.; Zhuravleva, M. Impurity-enhanced core valence luminescence via Zn-doping in cesium magnesium chlorides. *Optical Materials: X* **2024**, *24*, No. 100349.
(140) Voloshinovskii, A. S.; Mikhailik, V. B.; Rodnyi, P. A.; Pidzyrailo, S. N. Core-valance luminescence in CsBr-based crystals. *Jour Fizika Iverdogo Tela* **1992**, *34*, 2 (http://mi.mathnet.ru/ftt7360).
(141) Kubota, S.; Itoh, M.; Ruan, J.-Z.; Sakuragi, S.; Hashimoto, S. Observation of Interatomic Radiative Transition of Valence Electrons to Outermost-Core-Hole States in Alkali Halides. *Phys. Rev. Lett.* **1988**, *60*, 2319.
(142) Bertrand, G. H. V.; Hamel, M.; Sguerra, F. Current Status on Plastic Scintillators Modifications. *Chem. Eur. J.* **2014**, *20*, 15660.
(143) Zaitseva, N. P.; Glenn, A. M.; Mabe, A. N.; Carman, M. L.; Hurlbut, C. R.; Inman, J. W.; Payne, S. A. Recent developments in plastic scintillators with pulse shape discrimination. *Nuclear Instruments and Methods in physics Research Section A: Accelerators, Spectrometers, Detectors and Associated Equipment* **2018**, *889*, 97−104.
(144) Williamson, J. F.; Dempsey, J. F.; Kirov, A. S.; Monroe, J.; Binns, W. R.; Hedtjarn, H. Plastic scintillator response to low-energy photons. *Phys. Med. Biol.* **1999**, *44*, 857.
(145) Hajagos, T. J.; Liu, C.; Cherepy, N. J.; Pei, Q. High-Z Sensitized Plastic Scintillators: A Review. *Adv. Mater.* **2018**, *30*, 27.
(146) van Loef, E.; Markosyan, G.; Shirwadkar, U.; McClish, M.; Shah, K. Gamma-ray spectroscopy and pulse shape discrimination with a plastic scintillator. *Nuclear Instruments and Methods in physics Research Section A: Accelerators, Spectrometers, Detectors and Associated Equipment* **2015**, *788*, 71−72.
(147) Sato, A.; Magi, A.; Koshimizu, M.; Fujimoto, Y.; Kishimoto, S.; Asai, K. Photoluminescence and scintillation characteristics of Bi-loaded PVK-based plastic scintillators for the high counting-rate measurement of high-energy X-rays. *RSC Adv.* **2021**, *11*, 15581−15589.

(148) Wang, Y.; Li, M.; Chai, Z.; Wang, Y.; Wang, S. Perovskite Scintillators for Improved X-ray Detection and Imaging. *Angew. Chem.* **2023**, *62* (38), No. e202304638.
(149) Yan, W.; Duan, B.; Song, Y.; Song, G.; Ma, J.; Li, Y.; Li, B.; Liu, Y. Self-absorption and investigation of excited carrier dynamics in two-dimensional perovskite scintillator. *Appl. Phys. Lett.* **2024**, *124* (5), No. 053101.
(150) ter Weele, D. N.; Schaart, D. R.; Dorenbos, P. The Effect of Self-Absorption on the Scintillaton Properties of Ce^{3+} Activated $LaBr_3$ and $CeBr_3$. *IEEE Trans. Nucl. Sci.* **2014**, *61* (1), 683−688.
(151) van Dam, H. T.; Seifert, S.; Drozdowski, W.; Dorenbos, P.; Schaart, D. R. P[toca; Absorption Length, Scattering Length, and Refractive Index of $LaBr_3$:Ce^{3+}. *IEEE Trans. Nucl. Sci.* **2012**, *59* (3), 656−664.
(152) Alekhin, M. S., de Haas, J. T. M., Kramer, K. W., Khodyuk, I. V., de Vries, L., Dorenbos, P. Scintillation poperties and self absorption in SrI_2:Eu^{2+}, *IEEE Nuclear Science Symposium & Medical Imaging Conference*, 2010, DOI: 10.1109/NSSMIC.2010.5874044.
(153) Rutstrom, D.; Stand, L.; Koschan, M.; Melcher, c. L.; Zhuravleva, M. Europium concentration effects on the scintillation properties of Cs_4SrI_6:Eu and Cs_4CaI_6:Eu single crystals for use in gamma spectroscopy. *J. Lumin.* **2019**, *216*, 116740.
(154) van Aarle, C.; Roturier, N.; Biner, D. A.; Kramer, K. W.; Dorenbos, P. Light yield and thermal quenching of Ce^{3+} and Pr^{3+} co-doped $LaBr_3$:Sm^{2+} near-infrared scintillators. *Opt. Mater.* **2023**, *145*, 114375.
(155) Birowosuto, M. D.; Dorenbos, P.; van Eijk, C. W. E.; Kramer, K. W.; Gudel, H. U. $PrBr_3$: Ce^{3+}: A New Fast Lanthanide Trihalide Scintillator. *IEEE Trans. Nucl. Sci.* **2006**, *53*, 3028.
(156) Ueda, J.; Dorenbos, P.; Bos, A. J. J.; Meijerink, A.; Tanabe, S. Insight into the Thermal Quenching Mechanism for $Y_3Al_5O_{12}$:Ce^{3+} through Thermoluminescence Excitation Spectroscopy. *J. Phys. Chem. C* **2015**, *119*, 25003.
(157) Ueda, J. Analysis of optoelectronic properties and development of new persistent phosphor in Ce^{3+}-doped garnet ceramics. *Journal of the Ceramic Society of Japan* **2015**, *123*, 1059.
(158) Lin, Y.-C.; Bettinelli, M.; Karlsson, M. J. Preparation and luminescence properties of $Y_{3-y}Al_{5-x}Ga_xO_{12}$:$Ce^{3+}{}_y$ phosphors. *Chem. Mater.* **2019**, *31*, 3851.
(159) Jiang, L.; Zhang, X.; Zhu, S.; Tang, H.; Li, Q.; Zhang, W.; Mi, X.; Lu, L.; Liu, H.; Liu, X. *Journal of Materials Science: Materials in Electronics* **2018**, *29*, 9045.
(160) Dujardin, C.; Auffray, E.; Bourret-Courchesne, E.; Dorenbos, P.; Lecoq, P.; Nikl, M.; et al. Needs, Trend, and Advances in Inorganic Scintillators. *IEEE Trans. Nucl. Sci.* **2018**, *65* (8), 1977−1997.
(161) Aberg, D.; Sadigh, B.; Schleife, A.; Erhart, P. Origin of resolution enhancement by co-doping of scintillators: Insight from electronic structure calculations. *Appl. Phys. Lett.* **2014**, *104*, 211908.
(162) Yang, K., Menge, P. R., Buzniak, J. J., ouspenski, V. Performance improvement of large Sr^{2+} and Ba^{2+} co-doped $LaBr_3$:Ce^{3+} scintillation crystals, *IEEE Nuclear Science Symposium and Medical Imaging Conference Record (NSS/MIC)*, 2012, 308−311, DOI: 10.1109/NSSMIC.2012.6551113.
(163) Wu, Y.; Li, Q.; Rutstrom, D. J.; Greeley, I.; Stand, L.; Loyd, M.; Koschan, M.; Melcher, C. L. Effects of zirconium codoping on the optical and scintillation properties of SrI_2:Eu single crystals. *Nuclear Instruments and Methods in Physics Research Section A: Accelerators, Spectrometers, Detectors and Associated Equipment* **2020**, *954*, 161242.
(164) Wu, Y.; Li, Q.; rutstrom, D. J.; Zhuravleva, M.; Loyd, M.; Stand, l.; Koschan, M.; Melcher, C. L. Tailoring the Properties of Europium-Doped Potassium Calcium Iodide Scintillators Through Defect Engineering. *Physica Status Solidi Rapid Research Letters* **2018**, *12*, 1700403.
(165) Yamada, H.; Suzuki, A.; Uchida, Y.; Yoshida, M.; Yamamoto, H.; Tsukuda, Y. A Scintillator Gd_2O_2S:Pr, Ce, F, for X-ray Computed Tomography. *J. Electrochem. Soc.* **1989**, *136*, 2713.
(166) Nagarkar, V. V.; Brecher, C.; Ovechkina, E. E.; Gaysinskiy, V.; Miller, S. R.; Thacker, S.; et al. Scintillation Properties of CsI:Tl Crystals Codoped with Sm^{2+}. *IEEE Trans. Nucl. Sci.* **2008**, *55* (3), 1270−1274.
(167) Brecher, C.; Lempicki, A.; Miller, S. R.; Glodo, J.; Ovechkina, E. E.; Gaysinskiy, V.; Nagarkar, V. V.; Bartram, R. H. Suppression of afterglow in CsI:Tl by codoping with Eu^{2+} I: Experimental. *Nuclear Instruments and Methods in Physic Research Section A: Accelerators, Spectrometers, Detectors and Associated Equipment* **2006**, *558*, 450−457.
(168) Bartram, R. H.; Kappers, L. A.; Hamilton, D. S.; Lempicki, A.; Brecher, C.; Glodo, J.; Gaysinskiy, V.; Ovechkina, E. E. Suppression of afterglow in CsI:Tl by copding with Eu^{2+} II: Theoretical model. *Nuclear Instruments and Methods in Physic Research Section A: Accelerators, Spectrometers, Detectors and Associated Equipment* **2006**, *558*, 458−467.
(169) Totsuka, D.; Yanagida, T.; Fujimoto, Y.; Yokota, Y.; Moretti, F.; Vedda, A.; Yoshikawa, A. *Applied Physics Express* **2012**, *5* (5), 052601.
(170) Wu, Y.; Ren, G.; Meng, F.; chen, X.; Ding, D.; Li, H.; Pan, S. Effects of $Bi^{3.}$ doping on the optical and sicntillation properties of CsI:Tl single crystals. *Physica Status Solidi A* **2014**, *211*, 2586−2591.
(171) Wu, Y.; Ren, G.; Nikl, M.; Chen, X.; ding, D.; Li, H.; Pan, S.; Yang, F. CsI:Tl^+, Yb^{2+}: ultra-high light yield scintillator with reduced afterglow. *CrystEngComm* **2014**, *16*, 3312−3317.
(172) Yang, K.; Melcher, C. L.; Rack, P. D.; Eriksson, L. A. Effects of Calcium Codoping on Charge Traps in LSO:Ce Crystals. *IEEE Trans. Nucl. Sci.* **2009**, *56* (5), 2960−2965.
(173) Rothfuss, H. E.; Melcher, C. L.; Eriksson, L. A.; Spurrier Koschan, M. A. The effect of Cs^{2+} Codoping on Shallow Traps in YSO:Ce Scintillators. *IEEE Trans. Nucl. Sci.* **2009**, *56* (3), 958−961.
(174) Blahuta, S.; Bessiere, A.; Viana, B.; Dorenbos, P.; Ouspenski, V. Evidence and Consequences of Ce^{4+} in LYSO:Ce,Ca and LYSO:Ce,Mg Single Crystals for Medical Imaging Applications. *IEEE Trans. Nucl. Sci.* **2013**, *60* (4), 3134−3141.
(175) Kamada, K.; Yamaji, A.; Kurosawa, S.; Yokota, Y.; Ohashi, Y.; Yoshikawa, A. Mg co-doping effects on Ce doped $Y_3(Ga,Al)_5O_{12}$ scintillator. *IOP Conference Series: Materials Science and Engineering* **2017**, *169*, 012013.
(176) Nikl, M.; Kamada, K.; Babin, V.; Pejchal, J.; Pilarova, K.; Mihokova, E.; Beitlerova, A.; Bartosiewicz, K.; Kurosawa, S.; Yoshikawa, A. Defect Engineering in Ce-Doped Aluminum Garnet Single Crystal Scintilators. *Cryst. Growth Des.* **2014**, *14* (9), 4827−4833.
(177) Gerasymov, I.; Witkiewicz-Lukaszek, S.; Zorenko, T.; Bartosiewicz, K.; Zorenko, Y.; Winiecki, J. Effects of Codoping With Divalent Cations on Performance of YAG:Ce,C Scintillator. *IEEE Trans. Nucl. Sci.* **2023**, *70* (7), 1362−1369.
(178) Martinazzoli, L.; Nargelas, S.; Bohacek, P.; Cala, R.; Dusek, M.; Rohlicek, J.; Tamulaitis, G.; Auffray, E.; Nikl, M. Compositional engineering of multicomponent garnet scintillators: towards and ultra-accelerated scintillation response. *Materials Advances* **2022**, *3*, 6842−6852.
(179) Huang, X.; He, J.; Jiang, Y.; Chewpraditkul, W.; Zhang, L. Ultrafast GGAG:Ce X-ray scintillation ceramics with Ca^{2+} and Mg^{2+} co-dopants. *Ceram. Int.* **2022**, *48* (16), 23571−23577.
(180) Yu, D.; Wang, P.; Cao, F.; Gu, Y.; Liu, J.; Han, Z.; Huang, B.; Zou, Y.; Xu, X.; Zeng, H. Two-dimensional halide perovskties as β-ray scintillator for nuclear radiation monitoring. *Nat. Commun.* **2020**, *11*, 3395.
(181) Hardhienata, H.; Ahmad, F.; Arramel; Aminah, M.; Onggo, D.; Diguna, L. J.; Birowosuto, M. D.; Witkowski, M. E.; Makowski, M.; Drozdowski, W. Optical and X-ray scintillation properties of X_2MnCl_4 (X = PEA, PPA) perovskite crystals. *J. Phys. D: Appl. Phys.* **2020**, *53*, 455303.
(182) Zhou, Q.; Li, W.; Xiao, J.; Li, A.; Han, X. Low-Dimensional metal Halide for High Performance Scintillators. *Adv. Funct. Mater.* **2024**, *34* (38), 2402902.
(183) Shao, W.; Wang, X.; Zhang, Z.; Huang, J.; Han, Z.; Pi, S.; Xu, Q.; Zhang, X.; Xia, X.; Liang, H. Highly Efficient and Flexible Scintillation Screen Based on Manganese (II) Activated 2D Perovsktie for Planar and Nonplanar High-Resolution X-Ray Imaging, Advanced. *Opt. Mater.* **2022**, *10* (6), 2101182.

(184) Sheikh, M. A. K.; Kowal, D.; Mahyuddin, M. H.; Onggo, D.; Maddalena, F.; Dang, C.; Solution-Processable.; et al. A_2XY_4 (A = PEA, BA; X = Pb, Sn, Cu, Mn; Y = Cl, Br, I) Crystals for High Light Yield and Ultrafast Scintillators. *IEEE Trans. Nucl. Sci.* **2023**, *70*, 1384.
(185) Cala, R.; Frank, I.; Pagano, F.; Maddalena, F.; Dang, C.; Birowosuto, M. D.; Auffray, E. Sub-100-ps time resolution from undoped and Li-doped two-dimensional perovskite scintllators. *Applied physics Letters* **2022**, *120*, 24.
(186) Maddalena, F.; Mahyuddin, M. H.; Kowal, D.; Witkowski, M. E.; Makowski, M.; Sheikh, M. A. K.; Mahato, S.; Jedrzejewski, R.; Drozdowski, W.; Dujardin, C.; Dang, C.; Birowosuto, M. D. Lattice Expansion in Rb-Doped Hybrid Organic-Inorganic Perovskite Crystals Resulting in Smaller Band-Gap and Higher Light-Yield Scintillators. *Inorg. Chem.* **2023**, *62* (23), 8892−8902.
(187) Li, W.; Li, M.; he, Y.; Song, J.; Guo, K.; Pan, W.; Wei, h. Arising 2D Perovskites for Ionizing Radiation Detection. *Adv. Mater.* **2024**, *36* (26), 2309588.
(188) Sheikh, M. A. K.; Maddalena, F.; Kowal, D.; Makowski, M.; Mahato, S.; Jedrzejewski, R.; Bhattarai, R.; Witkowski, M. E.; Drozdowski, K. J.; Drozdowski, W.; Dang, C.; Rhone, T. D.; Birowosuto, M. D. Effect of Dual-Organic Cations on the Structure and Properties of 2D Hybrid Pervoskties as Scintillators. *ACS Appl. Mater. Interfaces* **2024**, *16*, 25529−25539.
(189) Sheikh, M. A. K.; Kowal, D.; Mahyuddin, M. H.; Cala', R.; Auffray, E.; Witkowski, M. E.; Makowski, M.; Drozdowski, W.; Wang, H.; Dujardin, C.; Cortecchia, D.; Birowosuto, M. D. $A_2B_{n-1}Pb_nI_{3n+1}$ (A = BA, PEA; B = MA; n = 1,2): Engineering Quantum-Well Crystals for High Mass Density and Fast Scintillators. *J. Phys. Chem. C* **2023**, *127* (22), 10737−10747.
(190) Moses, W. W.; Derenzo, S. E. Cerium fluoride, a new fast, heavy scintillator. *IEEE Trans. Nucl. Sci.* **1989**, *36*, 173−176.
(191) van Loef, E. V. D.; Dorenbos, P.; van Eijk, C. W. E.; Kramer, K.; Gudel, H. U. High-energy-resulution scintillator: Ce^{3+} activated $LaCl_3$. *Appl. Phys. Lett.* **2000**, *77*, 1467.
(192) Guillot-Noel, O.; De Haas, J. T. M.; Dorenbos, P.; van Eijk, C. W. E.; Kramer, K.; Güdel, H. U. Optical and scintillation properties of cerium-doped $LaCl_3$, $LuBr_3$ and $LuCl_3$. *J. Lumin.* **1999**, *85* (1−3), 21.
(193) Shah, K. S.; Glodo, J.; Klugerman, M.; Cirignano, L.; Moses, W. W.; Derenzo, S. E.; Weber, M. J. $LaCl_3$:Ce scintillator for y-ray detection. *Nuclear Instrumetns and Methods in Physics Research Section A: Accelerators, Spectrometers, Detectors and Associated Equipment* **2003**, *505*, 76.
(194) van Loef, E. V. D.; Dorenbos, P.; van Eijk, C. W. E.; Kramer, K. W.; Gudel, H. U. Properties and mechanism of scintillation in $LuCl_3$:Ce^{3+} and $LuBr_3$:Ce^{3+} crystals. *Nuclear Instrumetns and Methods in Physics Research Section A: Accelerators, Spectrometers, Detectors and Associated Equipment* **2003**, *496* (1), 138.
(195) Van't Spijker, J. C.; Dorenbos, P.; de Haas, J. T. M.; van Eijk, C. W. E.; Gudel, H. U.; Kramer, K. Scintillation properties of K_2LaCl_5 with Ce doping. *Radiat. Meas.* **1995**, *24* (4), 379.
(196) Roy, U. N.; Groza, M.; Cui, Y.; Burger, A.; Cherepy, N.; Friedrich, S.; Payne, S. A. K_2CeCl_5: A new scintillator material. *Nuclear Instruments and Methods in Physics Research Section A: Accelerators, Spectrometers, Detectors and Associated Equipment* **2007**, *579*, 46.
(197) Rooh, G.; Kang, H.; Kim, H. J.; Park, H.; Moon, J.; Lee, S.; Kim, S.; Kim, K. Study of the scintillation properties and of the proton induced radiation damage in the K_2CeCl_5 single crystal. *Journal of the Korean Physical Society* **2009**, *54*, 2093−2097.
(198) Zhuravleva, M.; Yang, K.; Green, A.; Melcher, C. L. Crystal growth and scintillation properties of Ce^{3+} doped KGd_2Cl_7. *J. Cryst. Growth* **2011**, *318*, 796.
(199) Fujimoto, Y.; Saeki, K.; Nakauchi, D.; Yanagida, T.; Koshimizu, M.; Asai, K. Characterisations of $CsSrCl_3$:Ce crystalline scintillator. *Sens. Mater.* **2017**, *29*, 1425.
(200) Gundiah, G.; Brennan, K.; Yan, Z.; Samulon, E. C.; Wu, G.; Bizarri, G. A.; Derenzo, S. E.; Bourret-Courchesne, E. D. Structure and scintillation properties of Ce^{3+}-activated $Cs_2NaLaCl_6$, Cs_3LaCl_6, $Cs_2NaLaBr_6$, Cs_3LaBr_6, Cs_2NaLaI_6 and Cs_3LaI_6. *J. Lumin.* **2014**, *149*, 374−384.
(201) Rooh, G.; Kang, H.; Kim, H. J.; Park, H.; Doh, S.-H.; kim, S. The growth and scintillation properties of $CsCe_2Cl_7$ crystal. *J. Cryst. Growth* **2008**, *311*, 128.
(202) Zhuravleva, M.; yang, K.; Melcher, C. L. Crystal growth and scintillation properties of Cs_3CeCl_6 and $CsCe_2Cl_7$. *J. Cryst. Growth* **2011**, *318*, 809.
(203) Samulon, E. C.; Gundiah, G.; Gascon, M.; Khodyuk, I. V.; Derenzo, S. E.; Bizarri, G. A.; Bourret-Courchesne, E. D. Luminescence and scintillation properties of Ce^{3+}-activated $Cs_2NaGdCl_6$, Cs_3GdCl_6, $Cs_2NaGdBr_6$ and Cs_3GdBr_6. *J. Lumin.* **2014**, *153*, 64−72.
(204) Kim, H. J.; Rooh, G.; Kim, S. Tl_2LaCl_5 (Ce^{3+}): New fast and efficient scintillator for X- and y-ray detection. *J. Lumin.* **2017**, *186*, 219−222.
(205) Hawrami, R.; Ariesanti, E.; Wei, H.; Finkelstein, J.; Glodo, J.; Shah, K. S. Tl_2LaCl_5:Ce, high performance scintillator for gamma-ray detectors Nuclear Instruments and Methods in Physics Research Section A: Accelerators, Spectrometers. *Detectors and Associated Equipment* **2017**, *869*, 107−109.
(206) Khan, A.; Rooh, G.; Kim, H. J.; Kim, S. Ce^{3+}-activated Tl_2GdCl_5: Novel halide scintillator for X-ray and y-ray detection. *J. Alloys Compd.* **2018**, *741*, 878−882.
(207) Rooh, G.; Kim, H. J.; Park, H.; Kim, S. Scintillation Characterization of $Rb_2LiCeCl_6$ Single Crystal. *IEEE Trans. Nucl. Sci.* **2012**, *59*, 2248.
(208) Rooh, G.; Kim, H. J.; Park, H.; Kim, S. Investigation of scintillation and luminescence properties of cerium doped $Rb_2LiGdCl_6$ single crystals. *J. Cryst. Growth* **2013**, *377*, 28−31.
(209) Combes, C. M.; Dorenbos, P.; van Eijk, C. W. E.; Kramer, K. W.; Gudel, H. U. Optical and scintillation properties of pure and Ce^{3+}-doped Cs_2LiYCl_6 and Li_3YCl_6:Ce^{3+} crystals. *J. Lumin.* **1999**, *82* (4), 299.
(210) Bessiere, A.; Dorenbos, P.; van Eijk, C. W. E.; Kramer, K. W.; Gudel, H. U. New thermal neutron scintillators: Cs_2LiYCl_6:Ce^{3+} and Cs_2LiYBr_6:Ce^{3+}. *IEEE Trans. Nucl. Sci.* **2004**, *51*, 2970.
(211) Glodo, J.; Hawrami, R.; van Loef, E.; Higgins, W.; Shirwadkar, U.; Shah, K. S. Dual gamma neutron detection with $Cs_2LiLaCl_6$, *Proceedings Volume 7449, Hard X-ray, Gamma-ray, and neutron detector physics XI:*, 2009, 74490E, .
(212) Rooh, G.; Kim, H. J.; Kim, S. Study on Crystal Growth and Scintillation Characteristics of $Cs_2LiCeCl_6$. *IEEE Trans. Nucl. Sci.* **2010**, *57*, 1255.
(213) Rooh, G.; kim, H. J.; Kim, S. Scintillation properties of $Cs_2LiGdCl_6$: Ce^{3+}. *Radiat. Meas.* **2010**, *45*, 412.
(214) Rooh, G.; Kang, H.; Kim, H. J.; Park, H.; Kim, S. The growth and scintillation properties of $Cs_2NaCeCl_6$ single crystal. *J. Cryst. Growth* **2009**, *311*, 2470.
(215) Rooh, G.; Kim, H. J.; Park, H.; Kim, S.; Jiang, H. Cerium-Doped $Cs_2NaGdCl_6$ Scintillator for X-Ray and y -Ray Detection. *IEEE Trans. Nucl. Sci.* **2014**, *61*, 397.
(216) Hawrami, R.; Ariesanti, E.; Soundara-Pandian, L.; Glodo, J.; Shah, K. S. Tl_2LiYCl_6:Ce: A New Elpasolite Scintillator. *IEEE Trans. Nucl. Sci.* **2016**, *63*, 2838.
(217) Kim, H. J.; Rooh, G.; Park, H.; Kim, S. Luminescence and scintillation properties of the new Ce-doped $Tl_2LiGdCl_6$ single crystals. *J. Lumin.* **2015**, *164*, 86−89.
(218) Rooh, G.; Kim, H. J.; Jang, J.; Kim, S. Scintillation characterizations of $Tl_2LiLuCl_6$: Ce^{3+} single crystal. *J. Lumin.* **2017**, *187*, 347−351.
(219) Selling, J.; Schweizer, S.; Birowosuto, M. D.; Dorenbos, P. Eu- or Ce-Doped Barium Halide Scintillators for X-Ray and y-Ray Detections. *IEEE Trans. Nucl. Sci.* **2008**, *55*, 1183.
(220) van Loef, E. V. D.; Dorenbos, P.; van Eijk, C. W. E.; Kramer, K.; Gudel, H. U. High-energy-resolution scintillator: Ce^{3+} activated $LaBr_3$. *Appl. Phys. Lett.* **2001**, *79*, 1573−1575.
(221) Bizarri, G.; Dorenbos, P. Charge carrier and exciton dynamics in $LaBr_3$:Ce^{3+} scintillators: Experiment and model. *Phys. Rev. B* **2007**, *75*, 184302.
(222) Birowosuto, M. D.; Dorenbos, P.; Kramer, K. W.; Gudel, H. U. Ce^{3+} activated $LaBr_{3-x}I_x$: High-light-yield and fast-response mixed halide scintillators. *J. Appl. Phys.* **2008**, *103*, 103517.

https://doi.org/10.1021/acs.chemmater.4c03437
Chem. Mater. 2025, 37, 1716−1740

(223) Shah, K. S.; Glodo, J.; Higgins, W.; van Loef, E. V. D.; Moses, W. W.; Derenzo, S. E.; Weber, M. J. $CeBr_3$ scintillators for gamma-ray spectroscopy. *IEEE Symposium Conference Record Nuclear Science* **2004**, 4278−4281.
(224) Drozdowski, W.; Dorenbos, P.; Bos, A. J. J.; Bizarri, G.; Owens, A.; Quarati, F. G. A. $CeBr_3$ scintillator development for possible use in space missions. *IEEE Trans. Nucl. Sci.* **2008**, *55*, 1391.
(225) Guss, P.; Foster, M. E.; Wong, B. M.; Doty, F. P.; Shah, K.; Squillante, M. R.; Shirwadkar, U.; Hawrami, R.; Tower, J.; Yuan, D. Results for aliovalent doping of $CeBr_3$ with Ca^{2+}. *J. Appl. Phys.* **2014**, *115*, 034908.
(226) Quarati, F. G. A.; Alekhin, M. S.; Kramer, K. W.; Dorenbos, P. Co-doping of $CeBr_3$ scintillator detectors for energy resolution enhancement, Nuclear Instruments and Methods in Physics Research Section A: Accelerators, Spectrometers. *Detectors and Associated Equipment* **2014**, *735*, 655−658.
(227) Awater, R. H. P.; Kramer, K. W.; Dorenbos, P. Effects of Na^+, Mg^{2+}, Ca^{2+}, Sr^{2+} and Ba^{2+} Doping on the Scintillation Properties of CeBr3. *IEEE Trans. Nucl. Sci.* **2015**, *62*, 2343.
(228) van Loef, E. V. D.; Dorenbos, P.; van Eijk, C. W. E.; Kramer, K. W.; Gudel, H. U. Optical and scintillation properties of pure and Ce^{3+} doped $GdBr_3$. *Opt. Commun.* **2001**, *189*, 297.
(229) van Loef, E. V. D.; Dorenbos, P.; van Eijk, C. W. E.; Kramer, K. W.; Gudel, H. U. Scintillation properties of K_2LaX_5:Ce^{3+} (X = Cl, Br, I). *Nuclear Instruments and Methods in Physics Research Section A: Accelerators, Spectrometers, Detectors and Associated Equipment* **2005**, *537*, 232.
(230) Kim, S.; Lee, J.; Doh, S.-H.; Kim, H. J.; Park, H.; Kang, H.; Kim, D.; U, H. Crystal Growth and Scintillation Properties of Rb_2CeBr_5. *IEEE Trans. Nucl. Sci.* **2009**, *56*, 982.
(231) Dorenbos, P.; van't Spijker, J. C.; Frijns, O. W. V.; van Eijk, C. W. E.; Kramer, K.; Gudel, H. U.; Ellens, A. Scintillation properties of $RbGd_2Br_7$:Ce^{3+} crystals; fast, efficient, and high density scintillators. *Nuclear Instruments and Methods in Physics Research Section A: Accelerators, Spectrometers, Detectors and Associated Equipment* **1997**, *132*, 728.
(232) Birowosuto, M. D.; Dorenbos, P.; van Eijk, C. W. E.; Kramer, K. W.; Gudel, H. U. Scintillation and luminescence properties of Ce^{3+} doped ternary cesium rare-earth halides. *Physica Statutus Solidi A Applications and Materials Science* **2007**, *204*, 850.
(233) Wu, Y.; Shi, H.; Chakoumakos, B. C.; Zhuravleva, M.; Du, M.-H.; Melcher, C. L. Crystal structure, electronic structure, temperature-dependent optical and scintillation properties of $CsCe_2Br_7$. *Journal of Materials Chemistry C* **2015**, *3*, 11366−11376.
(234) Kim, H. J.; Rooh, G.; Khan, A.; Kim, S. New Tl_2LaBr_5: Ce^{3+} crystal scintillator for y-rays detection. *Nuclear Instruments and Methods in Physics Research Section A: Accelerators, Spectrometers, Detectors and Associated Equipment* **2017**, *849*, 72−75.
(235) Birowosuto, M. D.; Dorenbos, P.; de Haas, J. T. M.; van Eijk, C. W. E.; Kramer, K. W.; Gudel, H. U. Thermal-Neutron scintillator: Ce^{3+} activated Rb_2LiYBr_6. *J. Appl. Phys.* **2007**, *101*, 6.
(236) Birowosuto, M. D.; Dorenbos, P.; de Haas, J. T. M.; van Eijk, C. W. E.; Kramer, K. W.; Gudel, H. U. Li-Based Thermal Neutron Scintillator Research; Rb_2LiYBr_6:Ce^{3+} and Other Elpasolites. *IEEE Trans. Nucl. Sci.* **2008**, *55*, 1152.
(237) Shirwadkar, U.; Glodo, J.; van Loef, E.; hawrami, R.; Mukhopadhyay, S.; Shah, K. S. Investigating scintillation properties of Ce doped Cs_2LiYBr_6. *IEEE Nuclear Science Symposium and Medical Imaging Conference* **2010**, 1585−1588.
(238) Glodo, J.; van Loef, E.; Hawrami, R.; Higgins, W. M.; Churilov, A.; Shirwadkar, U.; Shah, K. S. Selected Properties of Cs_2LiYCl_6, $Cs_2LiLaCl_6$, and $Cs_2LiLaBr_6$ Scintillators. *IEEE Trans. Nucl. Sci.* **2011**, *58*, 333.
(239) Qin, J.; Xiao, J.; Zhu, T.; Lu, X.; Han, Z.; Wang, M.; Jiang, L.; Mou, Y.; Sun, J.; Wen, Z.; Wang, X. Characteristic of a $Cs_2LiLaBr_6$:Ce scintillator detector and the responses for fast neutrons. *Nuclear Instruments and Methods in Physics Research Section A: Accelerators, Spectrometers, Detectors and Associated Equipment* **2018**, *905*, 112−118.
(240) Yang, K.; Menge, P. R.; Lejay, J.; Ouspenski, V. Scintillation properties and temperature responses of $Cs_2LiLaBr_6$:Ce3+. *IEEE Nuclear Science Symposium and Medical Imaging Conference* **2013**, 1−6.
(241) Cheon, J. K.; Kim, S.; Rooh, G.; So, J. H.; Kim, H. J.; Park, H. Scintillation characteristics of $Cs_2LiCeBr_6$ crystal. *Nuclear Instruments and Methods in Physics Research Section A: Accelerators, Spectrometers, Detectors and Associated Equipment* **2011**, *652*, 205.
(242) Rooh, G.; Kim, H. J.; Park, H.; Kim, S. Luminescence and scintillation characterizations of cerium doped $Cs_2LiGdBr_6$ single crystal. *J. Lumin.* **2014**, *146*, 404−407.
(243) Birowosuto, M. D.; Dorenbos, P.; van Eijk, C. W. E.; Kramer, K. W.; Gudel, H. U. Scintillation properties and anomalous Ce^{3+} emission of $Cs_2NaREBr_6$:Ce^{3+} (RE = La,Y,Lu). *J. Phys.: Condens. Matter* **2006**, *18*, 6133.
(244) Wei, H.; Stand, L.; Zhuravleva, M.; Meng, F.; Martin, V.; Melcher, C. L. Two new cerium-doped mixed-anion elpasolite scintillators: $Cs_2NaYBr_3I_3$ and $Cs_2NaLaBr_3I_3$. *Opt. Mater.* **2014**, *38*, 154−160.
(245) Kim, S.; Rooh, G.; Kim, H. J.; Kim, W.; hong, U. Crystal Growth and Scintillation Properties of $Cs_2NaCeBr_6$. *IEEE Trans. Nucl. Sci.* **2010**, *57*, 1251.
(246) Rooh, G.; Kim, H. J.; Park, H.; Kim, S. Luminescence and Scintillation Characterization of $Cs_2NaGdBr_6$: Ce^{3+} Single Crystal. *J. Lumin.* **2012**, *132*, 713.
(247) Kim, H. J.; Rooh, G.; Park, H.; Kim, S. Investigations of scintillation characterization of Ce-activated $Tl_2LiGdBr_6$ single crystal. *Radiat. Meas.* **2016**, *90*, 279−281.
(248) van Loef, E. V.; Higgins, W. M.; Glodo, J.; Churilov, A. V.; Shah, K. S. Crystal growth and characterization of rare earth iodides for scintillation detection. *J. Cryst. Growth* **2008**, *310*, 2090.
(249) Birowosuto, M. D.; Dorenbos, P.; Bizarri, G.; van Eijk, C. W. E.; Kramer, K. W.; Gudel, H. U. Temperature Dependent Scintillation and Luminescence Characteristics of GdI_3: Ce^{3+}. *IEEE Trans. Nucl. Sci.* **2008**, *55*, 1164.
(250) Birowosuto; Dorenbos, P.; van Eijk, C. W. E.; Kramer, K. W.; Gudel, H. U. Scintillation properties of LuI_3:Ce^{3+}-high light yield scintillators. *IEEE Trans. Nucl. Sci.* **2005**, *52*, 1114.
(251) Birowosuto, M. D.; Dorenbos, P.; van Eijk, C. W. E.; Kramer, K. W.; Gudel, H. U. High-light-output scintillator for photodiode readout: LuI_3:Ce^{3+}. *J. Appl. Phys.* **2006**, *99*, 123520.
(252) Shah, K. S.; Glodo, J.; Klugerman, M.; Higgins, W.; Gupta, T.; Wong, P.; Moses, W. W.; Derenzo, S. E.; Weber, M. J.; Dorenbos, P. LuI3:Ce a new scintillator for gamma ray spectroscopy. *IEEE Transactgions on Nuclear Science* **2004**, *51*, 2302.
(253) de Haas, J. T. M.; Dorenbos, P.; van Eijk, C. W. E. Measuring the absolute light yield of scintillators. *Nuclear Instruments and Methods in Physics Research Section A: Accelerators, Spectrometers, Detectors and Associated Equipment* **2005**, *537*, 97.
(254) Kapusta, M.; Balcerzyk, M.; Moszynski, M.; Pawelke, J. A high-energy resolution observed from a YAP:Ce scintillator, Nuclear Instruments and Methods in Physics Research Section A: Accelerators, Spectrometers. *Detectors and Associated Equipment* **1999**, *421* (3), 610.
(255) Dorenzo, S. E.; Weber, M. J.; Moses, W. W.; Dujardin, C. Measurements of the intrinsic rise times of common inorganic scintillators. *IEEE Trans. Nucl. Sci.* **2000**, *47*, 860−864.
(256) Moszynski, M.; Ludziejewski, T.; Wolski, D.; Klamra, W.; Norlin, L. O. Properties of the YAG:Ce scintillator. *Nuclear Instruments and Methods in physics Research Section A: Accelerators, Spectrometers, Detectors and Associated Equipment* **1994**, *345*, 461.
(257) Moszynski, M.; Wolski, D.; Ludziejewski, T.; Kapusta, M.; Lempicki, A.; Brecher, C.; Wisniewski, D.; Wojtowicz, A. J. Properties of the new LuAP:Ce scintillator. *Nuclear Instruments and Methods in Physics Research Section A: Accelerators, Spectrometers, Detectors and Associated Equipment* **1997**, *385*, 123.
(258) Mares, J. A.; Beitlerova, A.; Nikl, M.; Solovieva, N.; D'Ambrosio, C.; Blazek, K.; Maly, P.; Nejezchleb, K.; de Notaristefani, F. Scintillation response of Ce-doped or intrinsic scintillating crystals in the range up to 1 MeV. *Radiat. Meas.* **2004**, *38*, 353.

https://doi.org/10.1021/acs.chemmater.4c03437
Chem. Mater. 2025, 37, 1716−1740

(259) Balcerzyk, M.; Moszynski, M.; Kapusta, M.; Wolski, D.; Pawelke, J.; Melcher, C. L. YSO, LSO, GSO and LGSO. A study of energy resolution and nonproportionality. *IEEE Trans. Nucl. Sci.* **2000**, *47*, 1319.
(260) Cutler, P. A.; Melcher, C. L.; Spurrier, M. A.; Szupryczynski, P.; Eriksson, L. A. Scintillation Non-Proportionality of Lutetium- and Yttrium-Based Silicates and Aluminates. *IEEE Transations on Nuclear Science* **2009**, *56*, 915−919.
(261) Sakai, E. Recent Measurements on Scintillator-Photodetector Systems. *IEEE Trans. Nucl. Sci.* **1987**, *34*, 418.
(262) Kawamura, S.; Kaneko, J. H.; Higuchi, M.; Yamaguchi, T.; Haruna, J.; Yagi, Y.; Susa, K.; Fujita, F.; Homma, A.; Nishiyama, S.; Kurashige, K.; Ishibashi, H.; furusaka, M. Floating Zone Growth and Scintillation Characteristics of Cerium-Doped Gadolinium Pyrosilicate Single Crystals. *IEEE Trans. Nucl. Sci.* **2007**, *54*, 1383.
(263) Pidol, L.; Kahn-Harari, A.; Viana, B.; Virey, E.; Ferrand, B.; Dorenbos, P.; de Haas, J. T. M.; van Eijk, C. W. E. High efficiency of lutetium silicate scintillators, Ce-doped LPS, and LYSO crystals. *IEEE Trans. Nucl. Sci.* **2004**, *51*, 1084.
(264) Pauwels, D.; Le Masson, N.; Viana, B.; Kahn-Harari, A.; van Loef, E. V. D.; Dorenbos, P.; van Eijk, C. W. E. A novel inorganic scintillator: $Lu_2Si2O_7:Ce^{3+}$ (LPS). *IEEE Trans. Nucl. Sci.* **2000**, *47*, 1787.
(265) Wisniewski, D.; Wojtowicz, A. J.; Drozdowski, W.; Farmer, J. M.; Boatner, L. A. Scintillation and luminescence properties of Ce-activated $K_3Lu(PO_4)_2$. *J. Alloys Compd.* **2004**, *380*, 191.
(266) Holl, I.; Lorenz, E.; Mageras, G. A measurement of the light yield of common inorganic scintillators. *IEEE Trans. Nucl. Sci.* **1988**, *35*, 105.
(267) Menefee, J.; Swinehart, C. F.; O'Dell, E. W. Calcium Fluoride as an X-Ray and Charged Particle Detector. *IEEE Trans. Nucl. Sci.* **1966**, *13*, 720.
(268) Rajan, K. G.; Lenus, A. J. X-ray excited optical luminescence studies on the system BaXY (X,Y = F, Cl, Br, I). *Pramana Journal of Physics* **2005**, *65*, 323−338.
(269) Bourret-Courchesne, E. D.; Bizarri, G. A.; Borade, R.; Gundiah, G.; Samulon, E. C.; Yan, Z.; Derenzo, S. E. Crystal growth and characterization of alkali-earth halide scintillators. *J. Cryst. Growth* **2012**, *352*, 78.
(270) Yan, Z.; Bizarri, G.; Bourret-Courchesne, E. Scintillation properties of improved 5% Eu^{2+}-doped $BaCl_2$ single crystal for X-ray and y-ray detection. *Nuclear Instruments and Methods in Physics Research Section A: Accelerators, Spectrometers, Detectors and Associated Equipment* **2013**, *698*, 7.
(271) Zhuravleva, M.; Blalock, B.; Yang, K.; Koschan, M.; Melcher, C. L. New single crystal scintillators: $CsCaCl_3$:Eu and $CsCaI_3$:Eu. *J. Cryst. Growth* **2012**, *352*, 115.
(272) Cherginets, V. L.; Rebrova, N. V.; Grippa, A. Y.; Datsko, y. N.; Ponomarenko, T. V.; Pedash, V. Y.; Kosinov, N. N.; Tarasov, V. A.; Zelenskaya, O. V.; Zenya, I. M.; Lopin, A. V. Scintillation properties of $CsSrX_3:Eu^{2+}$ ($CsSr_{1-y}Eu_yX_3$, X = Cl, Br; $0 \leq y \leq 0.05$) single crystal grown by the Bridgman method. *Mater. Chem. Phys.* **2014**, *143*, 1296.
(273) Stand, L.; Zhuravleva, M.; Chakoumakos, B.; Wei, H.; Johnson, J.; Martin, V.; Loyd, M.; Rutstrom, D.; McAlexander, W.; Wu, Y.; Koschan, M.; Melcher, C. L. Characterization of mixed halide scintillators: $CsSrBrI_2$:Eu, $CsCaBrI_2$:Eu and $CsSrClBr_2$:Eu. *J. Lumin.* **2019**, *207*, 70−77.
(274) Grippa, A.Y..; Rebrova, N.V.; Gorbacheva, T.E.; Pedash, V.Y.; Kosinov, N.N.; Cherginets, V.L.; Tarasov, V.A.; Tarasenko, O.A. Scintillation properties of $CaBr_2$ crystals doped with Eu^{2+} ions. *Nuclear Instruments and Methods in Physics Research Section A: Accelerators, Spectrometers, Detectors and Associated Equipment* **2013**, *729*, 356−359.
(275) Yan, Z.; Gundiah, G.; Bizarri, G. A.; Samulon, E. C.; Derenzo, S. E.; Bourret-Courchesne, E. D. Eu^{2+}-activated $BaCl_2$, $BaBr_2$ and BaI_2 scintillators revisited. *Nuclear Instruments and Methods in Physics Research Section A: Accelerators, Spectrometers, Detectors and Associated Equipment* **2014**, *735*, 83−87.
(276) Bizarri, G.; Bourret-Courchesne, E. D.; Yan, Z.; Derenzo, S. E. Scintillation and Optical Properties of BaBrI:Eu^{2+} and $CsBa_2I_5:Eu^{2+}$. *IEEE Trans. Nucl. Sci.* **2011**, *58*, 3403.
(277) Bourret-Courchesne, E. D.; Bizarri, G.; Hanrahan, S. M.; Gundiah, G.; Yan, Z.; Derenzo, S. E. BaBrI:Eu^{2+}, a new bright scintillator. *Nuclear Instruments and Methods in Physics Research Section A: Accelerators, Spectrometers, Detectors and Associated Equipment* **2010**, *613*, 95.
(278) Soundara-Pandian, L.; Hawrami, R.; Glodo, J.; Ariesanti, E.; van Loef, E. V.; Shah, K. Lithium Alkaline Halides−Next Generation of Dual Mode Scintillators. *IEEE Trans. Nucl. Sci.* **2016**, *63*, 490.
(279) Stand, L.; Zhuravleva, M.; Wei, H.; Melcher, C. L. Crystal growth and scintillation properties of potassium strontium bromide. *Opt. Mater.* **2015**, *46*, 59−63.
(280) Pestovich, K. S.; Stand, L.; van Loef, E.; Melcher, C. L.; Zhuravleva, M. Crystal Growth and Characterization of Europium-Doped Rubidium Calcium Bromide Scintillators. *IEEE Trans. Nucl. Sci.* **2023**, *70*, 1370.
(281) Stand, L.; Zhuravleva, M.; Johnson, J.; Koschan, M.; Lukosi, E.; Melcher, C. L. New high performing scintillators: $RbSr_2Br_5$:Eu and $RbSr_2I_5$:Eu. *Opt. Mater.* **2017**, *73*, 408−414.
(282) Grippa, A. Y.; Rebrova, N. V.; Gorbacheva, T. E.; Pedash, V. Y.; Kosinov, N. N.; Cherginets, V. L.; Tarasov, V. A.; Tarasenko, O. A.; Lopin, A. V. Crystal growth and scintillation properties of $CsCaBr_3:Eu^{2+}$ ($CsCa_{1-x}Eu_xBr$, $0 \leq x \leq 0.08$. *J. Cryst. Growth* **2013**, *371*, 112−116.
(283) Loyd, M.; Lindsey, A.; Stand, L.; Zhuravleva, M.; Melcher, C. L.; Koschan, M. Tuning the structure of $CsCaI_3$:Eu via substitution of bromine for iodine. *Eu via substitution of bromine for iodine* **2017**, *68*, 47−52.
(284) Gokhale, S. S.; Stand, L.; Lindsey, A.; Koschan, M.; Zhuravleva, M.; Melcher, C. L. Improvement in the optical quality and energy resolution of $CsSrBr_3$:Eu scintillator crystals. *J. Cryst. Growth* **2016**, *445*, 1−8.
(285) Syntfeld, A.; Moszynski, M.; Arlt, R.; Balcerzyk, M.; Kapusta, M.; Majorov, M.; Marcinkowski, R.; schotanus, P.; Swoboda, M.; Wolski, D. ^{6}Li(Eu) in neutron and gamma-ray spectrometry - a highly sensitive thermal neutron detector. *IEEE Trans. Nucl. Sci.* **2005**, *52*, 3151.
(286) Yasumune, T.; Kurihara, M.; Maehata, K.; Iyomoto, N.; Ishibashi, K. Scintillation Properties of ^{6}LiI(Eu) in Cryogenic Temperatures. *Journal of Low Temperature Physics* **2012**, *167*, 442−446.
(287) Hofstadter, R.; O'Dell, E. W.; Schmidt, C. T. CaI_2 and CaI_2(Eu) Scintillation Crystals. *IEEE Trans. Nucl. Sci.* **1964**, *11*, 12.
(288) Boatner, L. A.; Ramey, J. O.; kolopus, J. A.; Neal, J. S. Divalent europium doped and un-doped calcium iodide scintillators: Scintillator characterization and single crystal growth. *Nuclear Instruments and Methods in Physics Research Section A: Accelerators, Spectrometers, Detectors and Associated Equipment* **2015**, *786*, 23−31.
(289) Kamada, K.; chiba, H.; Yoshino, M.; Yamaji, A.; Shoji, Y.; Kurosawa, S.; Yokota, Y.; Ohashi, Y.; Yoshikawa, A. Growth and scintillation properties of Eu doped $LiSrI_3$/LiI eutectics. *Opt. Mater.* **2017**, *68*, 70−74.
(290) Lindsey, A. C.; Zhuravleva, M.; Stand, L.; Wu, Y.; Melcher, C. L. Crystal growth and characterization of europium doped $KCaI_3$, a high light yield scintillator. *Opt. Mater.* **2015**, *48*, 1−6.
(291) Wu, Y.; Li, Q.; Chakoumakos, B. C.; Zhuravleva, M.; Lindsey, A. C.; Johnson, J. A.; Stand, L.; Koschan, M.; Melcher, C. L. Quaternary Iodide K(Ca,Sr)$I_3:Eu^{2+}$ Single-Crystal Scintillators for Radiation Detection: Crystal Structure, Electronic Structure, and Optical and Scintillation Properties. *Advanced Optical Materials* **2016**, *4*, 1518.
(292) Stand, L.; Zhuravleva, M.; Lindsey, A.; Melcher, C. L. Growth and characterization of potassium strontium iodide: A new high light yield scintillator with 2.4% energy resolution. *Spectrometers, Detectors and Associated Equipment* **2015**, *780*, 40−44.
(293) Stand, L.; Zhuravleva, M.; Chakoumakos, B.; Johnson, J.; Lindsey, A.; Melcher, C. L. Scintillation properties of Eu^{2+}-doped KBa_2I_5 and K_2BaI_4. *Journal of Lumienscence* **2016**, *169*, 301−307.

https://doi.org/10.1021/acs.chemmater.4c03437
Chem. Mater. 2025, 37, 1716−1740

(294) Pestovich, K. S.; Stand, L.; Melcher, C. L.; van Loef, E.; Zhuravleva, M. Crystal growth of new high light yield halide perovskite scintillator $RbSrI_3$. *J. Cryst. Growth* **2024**, *627*, 127540.
(295) Johnson, J. A.; Zhuravleva, M.; Stand, L.; Chakoumakos, B. C.; Wu, Y.; Greely, I.; rutstrom, D.; Koschan, M.; Melcher, C. L. Discovery of New Compounds and Scintillators of the A_4BX_6 Family: Crystal Structure, Thermal, Optical, and Scintillation Properties. *Cryst. Growth Des.* **2018**, *18*, 5220.
(296) Stand, L.; Zhuravleva, M.; Chakoumakos, B.; Johnson, J.; Loyd, M.; Wu, Y.; Koschan, M.; Melcher, C. L. Crystal Growth and Scintillation Properties of Eu^{2+} doped Cs_4CaI_6 and Cs_4SrI_6. *J. Cryst. Growth* **2018**, *486*, 162.
(297) Kim, H. J.; Rooh, G.; Khan, A.; Park, H.; Kim, S. Scintillation performance of the $TlSr_2I_5$ (Eu^{2+}) single crystal. *Opt. Mater.* **2018**, *82*, 7−10.
(298) Glodo, J., Farrell, R., van Loef, E. V. D., Higgins, W. M., Shah, K. S. $LaBr_3$:Pr^{3+} - a new red-emitting scintillator, *IEEE Nuclear Science Symposium conference Record*, 2005, DOI: 10.1109/NSSMIC.2005.1596215.
(299) Mares, J. A.; Nikl, M.; Beitlerova, A.; Horodysky, P.; Blazek, K.; Bartos, K.; D'Ambrosio, C. Scintillation properties of Ce^{3+}- and Pr^{3+}-doped LuAG, YAG and mixed $Lu_xY_{1-x}AG$ garnet crystals. *IEEE Trans. Nucl. Sci.* **2012**, *59*, 2120.
(300) Drozdowski, W.; Brylew, K.; Wojtowicz, A. J.; Kisielewski, J.; Swirkowicz, M.; Lukasiewicz, T.; de Haas, J. T. M.; Dorenbos, P. 33000 photons per MeV from mixed $(Lu_{0.75}Y_{0.25})_3Al_5O_{12}$:Pr scintillator crystals. *Optical Materials Express* **2014**, *4*, 1207.
(301) Foster, C.; Wu, Y.; Koschan, M.; Melcher, C. L. Improvements in Light Yield and Energy Resolution by Li^+ Codoping $(Lu_{0.75}Y_{0.25})_3Al_5O_{12}$:$Pr^{3+}$ Single Crystal Scintillators. *Physica Status Solidi Rapid Research Letters* **2018**, *12*, 9.
(302) Yang, K.; Menge, P. R. Improving y-ray energy resolution, non-proportionality, and decay time of NaI:Tl^+ with Sr^{2+} and Ca^{2+} co-doping. *J. Appl. Phys.* **2015**, *118*, 21.
(303) Khodyuk, I. V.; Messina, S. A.; Hayden, T. J.; Bourret, E. D.; Bizarri, G. A. Optimization of scintillation performance via a combinatorial multi-element co-doping strategy: Application to NaI:Tl. *J. Appl. Phys.* **2015**, *118*, 8.
(304) Shiran, N. V.; Gektin, A. V.; Boyarintseva, Y.; Vasyukov, S.; Boyarintsev, A.; Pedash, V.; Tkachenko, S.; Zelenskaya, O.; Kosinov, N.; Kisil, O.; Philippovich, L. Eu Doped and Eu, Tl Co-Doped NaI Scintillators. *IEEE Trans. Nucl. Sci.* **2010**, *57*, 1233.
(305) Syntfeld-Kazuch, A.; Swiderski, L.; Czarnacki, W.; Gierlik, M.; Klamra, W.; Moszynski, M.; Schotanus, P. Non-Proportionality and Energy Resolution of CsI(Tl). *IEEE Trans. Nucl. Sci.* **2007**, *54*, 1836.
(306) Rowe, E.; Bhattacharya, P.; Tupitsyn, E.; Groza, M.; Burger, A.; Cherepy, N. J.; Payne, S. A.; Sturm, B. W.; Pedrini, C. A New Lanthanide Activator for Iodide Based Scintillators: Yb^{2+}. *IEEE Trans. Nucl. Sci.* **2013**, *60*, 1057.
(307) Selling, J.; Birowosuto, M. D.; Dorenbos, P.; Schweizer, S. Europium-doped barium halide scintillators for x-ray and y-ray detections. *J. Appl. Phys.* **2007**, *101*, 3.
(308) Burger, A.; Rowe, E.; Groza, M.; Morales Figueroa, K.; Cherepy, N. J.; Beck, P. R.; Hunter, S.; Payne, S. A. Cesium hafnium chloride: A high light yield, non-hygroscopic cubic crystal scintillator for gamma spectroscopy. *Appl. Phys. Lett.* **2015**, *107*, 14.
(309) van Blaaderen, J. J.; Maddalena, F.; Dang, C.; Birowosuto, M. D.; Dorenbos, P. Temperature dependent scintillation properties and mechanisms of $(PEA)_2PbBr_4$ single crystals. *Journal of Materials Chemistry C* **2022**, *10*, 11598−11606.
(310) van Loef, E.; Pandian, L. S.; Kaneshige, N.; Ciampi, G.; Stand, L.; Rutstrom, D.; Tratsiak, Y.; Zhuravleva, M.; Melcher, C.; Shah, K. S. Crystal Growth, Density Functional Theory, and Scintillation Properties of $TlCaX_3$ (X = Cl, Br, I). *IEEE Trans. Nucl. Sci.* **2023**, *70*, 1378.
(311) Rooh, G.; Khan, A.; Kim, H. J.; Park, H.; Kim, S. $TlSr_2Br_5$: New intrinsic scintillator for X-ray and y-ray detection. *Opt. Mater.* **2017**, *73*, 523−526.
(312) Iida, T.; Kamada, K.; Yoshino, M.; kim, K. J.; Ichimura, K.; Yoshikawa, A. High-light-yield calcium iodide (CaI_2) scintillator for astroparticle physics. *Nuclear Instruments and Methods in Physics Research Section A: Accelerators, Spectrometers, Detectors and Associated Equipment* **2020**, *958*, 162629.
(313) Fukabori, A.; An, L.; Ito, A.; Chani, V.; Kamada, K.; Goto, T.; Yoshikawa, A. Scintillation Characteristics of Undoped Sc_2O_3 Single Crystals and Ceramics. *IEEE Trans. Nucl. Sci.* **2012**, *59*, 2594.
(314) Mikhailik, V. B.; Kraus, H.; Henry, S.; Tolhurst, A. J. B. Scintillation studies of $CaWO_4$ in the millikelvin temperture range. *Phys. Rev. B* **2007**, *75*, 184308.
(315) Zdesenko, Y. G.; Avignone, F. T., III; Brudanin, V. B.; Danevich, F.; Nagorny, S. S.; Solsky, I. M.; Tretyak, V. I. Scintillation properties and radioactive contamination of $CaWO_4$ crystal scintillators. *Nuclear Instruments and Methods in Physics Research Section A: Accelerators, Spectrometers, Detectors and Associated Equipment* **2005**, *538*, 657.
(316) Moszynski, M.; Balcerzyk, M.; Czarnacki, W.; Nassalski, A.; Szczęśniak, T.; Kraus, H.; Mikhailik, V. B.; Solskii, I. M. Characterization of $CaWO_4$ scintillator at room and liquid nitrogen temperatures. *Nuclear Instruments and Methods in Physics Research Section A: Accelerators, Spectrometers, Detectors and Associated Equipment* **2005**, *553*, 578.
(317) Melcher, C. L.; Manente, R. A.; Schweitzer, J. S. Applicability of barium fluoride and cadmium tungstate scintillators for well logging. *IEEE Transactions on Nclear Science* **1989**, *36*, 1188.
(318) Annenkov, A. A.; Korzhik, M. V.; Lecoq, P. Lead tungstate scintillation material. *Nuclear Instruments and Methods in Physics Research Section A: Accelerators, Spectrometers, Detectors and Associated Equipment* **2002**, *490*, 30.
(319) Kobayashi, M.; Ishii, M.; Usuki, Y.; Yahagi, H. Scintillation characteristics of $PbWO_4$ single crystals at room temperature. *Nuclear Instruments and Methods in Physics Research Section A: Accelerators, Spectrometers, Detectors and Associated Equipment* **1993**, *333*, 429.
(320) Grabmaier, B. C. Crystal Scintillators. *IEEE Trans. Nucl. Sci.* **1984**, *31*, 372.
(321) De Notaristefani, F., Lecoq, P., Schneegans, M. *Proceedings of the Cristal 2000 international workshop (Heavy Scintillators for Scientific and Industrial Applications*, 1992, ISBN: 2-86332-128-5.
(322) Laval, M.; Moszynski, M.; Allemand, R.; Cormoreche, E.; Guinet, P.; Odru, R.; Vacher, J. Barium fluoride − Inorganic scintillator for subnanosecond timing. *Nuclear Instruments and Methods in physics Reserach* **1983**, *206*, 169.
(323) Biasini, M.; Cassidy, D. B.; Deng, S. H. M.; Tanaka, H. K. M.; Mills, A. P. Suppression of the slow component of scintillation light in BaF_2. *Nuclear Instruments and Methods in Physics Research Section A: Accelerators, Spectrometers, Detectors and Associated Equipment* **2005**, *553*, 550.
(324) Nanal, V.; Back, B. B.; Hofman, D. J. Temperature dependence of BaF_2 scintillation. *Nuclear Instruments and Methods in Physics Research Section A: Accelerators, Spectrometers, Detectors and Associated Equipment* **1997**, *389*, 430.
(325) Moszynski, M.; Allemand, R.; Laval, M.; Odru, R.; Vacher, J. Recent progress in fast timing with CsF scintillators in application to time-of-flight positron tomography in medicine. *Nucl. Instrum. Methods Phys. Res.* **1983**, *205*, 239.
(326) Yamanoi, K.; Nishi, R.; Takeda, K.; Shinzato, Y.; Tsuboi, M.; Luong, M. V.; Nakazato, T.; Shimizu, T.; Sarukura, N.; Cadatal-Raduban, M.; Pham, M. H.; Nguyen, H. D.; Kurosawa, S.; Yokota, Y.; Yoshikawa, A.; Togashi, T.; Nagasono, M.; Ishikawa, T. Perovskite fluoride crystals as light emitting materials in vacuum ultraviolet region. *Opt. Mater.* **2014**, *36*, 769.
(327) Koshimizu, M.; Yahaba, N.; Haruki, R.; Nishikido, F.; Kishimoto, S.; Asai, K. Scintillation and luminescence properties of a single $CsCaCl_3$ crystal. *Opt. Mater.* **2014**, *36*, 1930.
(328) Jansons, J.; Rachko, Z.; Valbis, J.; Andriessen, J.; Dorenbos, P.; van Eijk, C. W. E.; Khaidukov, N. M. Cross-luminescence of complex halide crystals. *J. Phys.: Condens. Matter* **1993**, *5*, 1589.
(329) Yanagida, T.; Watanabe, K.; Fujimoto, Y. Comparative study of neutron and gamma-ray pulse shape discrimination of anthracene, stilbene, and p-terphenyl. *Nuclear Instruments and Methods in Physics*

Research Section A: Accelerators, Spectrometers, Detectors and Associated Equipment **2015**, *784*, 111−114.
(330) Birks, J. B. The Fluorescence and Scintillation Decay Times of Crystalline Anthracene. *Proceedings of the Physical Society* **1962**, *79*, 494.
(331) Post, R. F.; Shiren, N. S. Decay Time of Stilbene Scintillations as a Function of Temperature. *Physical Review Journals Archive* **1950**, *78*, 80.
(332) De Gerone, M.; Biasotti, M.; Ceriale, V.; Corsini, D.; Gatti, F.; Orlando, A.; Pizzigoni, G. Properties of single crystal para-terphenyl as medium for high resolution TOF detector. *Nuclear Instruments and Methods in Physics Research Section A: Accelerators, Spectrometers, Detectors and Associated Equipment* **2016**, *824*, 192−193.
(333) Rupert, B. L.; Cherepy, N. J.; Sturm, B. W.; Sanner, R. D.; Payne, S. A. Bismuth-loaded plastic scintillators for gamma-ray spectroscopy. *Europhys. Lett.* **2012**, *97*, 22002.
(334) Data Sheet Luxium Solutions BC-400, Accessed 24 March 2024. https://luxiumsolutions.com/radiation-detection-scintillators/plastic-scintillators/bc400-bc404-bc408-bc412-bc416.
(335) Data Sheet Luxium Solutions BC-408, Accessed 24 March 2024. https://luxiumsolutions.com/radiation-detection-scintillators/plastic-scintillators/bc400-bc404-bc408-bc412-bc416.
(336) Data Sheet Luxium Solutions BC-412, Accessed 24 March 2024. https://luxiumsolutions.com/radiation-detection-scintillators/plastic-scintillators/bc400-bc404-bc408-bc412-bc416.
(337) Data Sheet Luxium Solutions BC-428, Accessed 24 March 2024. https://luxiumsolutions.com/radiation-detection-scintillators/plastic-scintillators/greenemitting-bc-428.
(338) Data Sheet Luxium Solutions BC-430, Accessed 24 March 2024. https://luxiumsolutions.com/radiation-detection-scintillators/plastic-scintillators/redemitting-bc-430.
(339) Data Sheet Luxium Solutions Lead Loaded BC-452, Accessed 24 March 2024. https://luxiumsolutions.com/radiation-detection-scintillators/plastic-scintillators/leadloaded-bc-452.
(340) Data Sheet Eljen Technology EJ-200, Accessed 24 March 2024. https://eljentechnology.com/products/plastic-scintillators/ej-200-ej-204-ej-208-ej-212.
(341) Data Sheet Eljen Technology EJ-240, Accessed 24 March 2024. https://eljentechnology.com/products/plastic-scintillators/ej-240.
(342) Data Sheet Eljen Technology EJ-260, Accessed 24 March 2024. https://eljentechnology.com/products/plastic-scintillators/ej-260-ej-262.
(343) Data Sheet Eljen Technology Lead Loaded EJ-256, Accessed 24 March 2024. https://eljentechnology.com/products/plastic-scintillators/ej-256.

https://doi.org/10.1021/acs.chemmater.4c03437
Chem. Mater. 2025, 37, 1716−1740